Astronomy & Astrophysics manuscript no. 12414
August 18, 2009
© ESO 2009

arXiv:0908.2539v1 [astro-ph.CO] 18 Aug 2009

An investigation of the luminosity-metallicity relation for a large sample of low-metallicity emission-line galaxies ⋆, ⋆⋆

N. G. Guseva[1,2], P. Papaderos[3,4], H. T. Meyer[5,6], Y. I. Izotov[1,2], and K. J. Fricke[1]

[1] Max-Planck-Institute for Radioastronomy, Auf dem Hügel 69, 53121 Bonn, Germany
[2] Main Astronomical Observatory, Ukrainian National Academy of Sciences, Zabolotnoho 27, Kyiv 03680, Ukraine
[3] Instituto de Astrofísica de Andalucía (CSIC), Camino Bajo de Huétor 50, Granada E-18008, Spain
[4] Department of Astronomy and Space Physics, Uppsala University, Box 515, SE-75120 Uppsala, Sweden
[5] Astronomisches Rechen-Institut am Zentrum für Astronomie (ZAH), Mönchhofstr. 12-14, 69120 Heidelberg, Germany
[6] Institute for Astrophysics, University of Göttingen, Friedrich-Hund-Platz 1, 37077 Göttingen, Germany

Received ; Accepted

ABSTRACT

Context. We present 8.2m VLT spectroscopic observations of 28 H II regions in 16 emission-line galaxies and 3.6m ESO telescope spectroscopic observations of 38 H II regions in 28 emission-line galaxies. These emission-line galaxies were selected mainly from the Data Release 6 (DR6) of the Sloan Digital Sky Survey (SDSS) as metal-deficient galaxy candidates.
Aims. We collect photometric and high-quality spectroscopic data for a large uniform sample of star forming galaxies including new observations. Our aim is to study the luminosity-metallicity ($L - Z$) relation for nearby galaxies, especially at its low-metallicity end and compare it with that for higher-redshift galaxies.
Methods. Physical conditions and element abundances in the new sample are derived with the T_e-method, excluding six H II regions from the VLT observations and nearly two third of the H II regions from the 3.6m observations. Element abundances for the latter galaxies were derived with the semiempirical strong-line method.
Results. From our new observations we find that the oxygen abundance in 61 out of the 66 H II regions of our sample ranges from 12 + log O/H = 7.05 to 8.22. Our sample includes 27 new galaxies with 12 + log O/H < 7.6 which qualify as extremely metal-poor star-forming galaxies (XBCDs). Among them are 10 H II regions with 12 + log O/H < 7.3. The new sample is combined with a further 93 low-metallicity galaxies with accurate oxygen abundance determinations from our previous studies, yielding in total a high-quality spectroscopic data set of 154 H II regions. 9000 more galaxies with oxygen abundances, based mainly on the T_e-method, are compiled from the SDSS. Photometric data for all galaxies of our combined sample are taken from the SDSS database while distances are from the NED. Our data set spans a range of 8 mag with respect to its absolute magnitude in SDSS g ($-12 \gtrsim M_g \gtrsim -20$) and nearly 2 dex in its oxygen abundance ($7.0 \lesssim 12 + \log \mathrm{O/H} \lesssim 8.8$), allowing us to probe the $L - Z$ relation in the nearby universe down to the lowest currently studied metallicity level. The $L - Z$ relation established on the basis of the present sample is consistent with previous ones obtained for emission-line galaxies.

Key words. galaxies: fundamental parameters – galaxies: starburst – galaxies: abundances

1. Introduction

It was shown more than 20 years ago that low-luminosity dwarf galaxies have systematically lower metallicities compared to more luminous galaxies (Lequeux et al. , 1979; Skillman et al. , 1989; Richer & McCall , 1995). This dependence, initially obtained for irregular galaxies, was later confirmed for galaxies of different morphological types (e.g. Vila-Costas & Edmunds , 1992; Kobulnicky & Zaritsky , 1999; Melbourne & Salzer , 2002; Lee et al. , 2004; Pilyugin et al. , 2004; Lee et al. , 2006).

The differences between giant and dwarf galaxies are usually attributed to different chemical evolution of galaxies with different masses (e.g. Lequeux et al. , 1979; Tremonti et al. , 2004; Lee et al. , 2006; Ellison et al. , 2008; Gavilán et al. , 2009). Thus, more efficient mechanisms seem to be at work in massive galaxies converting gas into stars and/or less efficient ones ejecting enriched matter into the galactic halo or even into the intergalactic medium. While the mass of a galaxy is one of the key physical parameters governing galaxy evolution, its determination is not easy and somewhat uncertain. Therefore, very often the luminosity, which is directly derived from observations, is used instead of the mass. In addition, some authors also use other global characteristics of a galaxy such as Hubble morphological type, rotation velocity, the gas mass fraction, surface brightness of the galaxy, to study correlations between metallicity and macroscopic properties of a galaxy (e.g. Tremonti et al. , 2004; Pilyugin et al. , 2004).

Metallicity reflects the level of the gas astration in the galaxy. Hence, the metallicity of a galaxy depends strongly on its evolutionary state, specifically, on the fraction of the gas converted into stars. The metallicity in emission-line galaxies is defined in terms of the relative abundance of oxygen to hydrogen (usually 12 + log O/H) in the interstellar medium (ISM). Different mechanisms were considered in chemical evolution models to account for the low metallicity of dwarf galaxies, mainly 1) enriched galactic wind outflow which expells the newly synthe-

Send offprint requests to: N.G. Guseva, guseva@mao.kiev.ua

⋆ Based on observations collected at the European Southern Observatory, Chile, VLT and 3.6m telescopes.

⋆⋆ Tables 1 - 6 and Figures 1 - 2 are only available in electronic form in the online edition.

sized heavy elements from the galaxy, resulting in slowing enrichment of the galaxy ISM; 2) inflow of metal-poor intergalactic gas and its mixing with the galaxy ISM which results in decreasing ISM metallicity, and 3) the burst character of star formation with a very low level of astration between the bursts. In principle, chemical evolution models could predict the slope and scatter of the mass-metallicity $M - Z$ (and luminosity-metallicity $L - Z$) relations over a large range in mass (luminosity) and metallicity invoking the mechanisms mentioned above.

Usually, $L - Z$ relations are based on optical observations of nearby galaxies. However, it was shown in recent studies that the near infrared (NIR) range could be more promising for such studies. Saviane et al. (2008) collected abundances obtained by means of the temperature-sensitive method and NIR luminosities for a sample of dwarf irregular galaxies with $-20 < M_H < -13$, located in nearby groups of galaxies. They obtained a tight $M - Z$ relation with a low scatter of 0.11 dex around its linear fit. Salzer et al. (2005) (see also Vaduvescu et al. , 2007) noted that the NIR luminosities are more fundamental than the *B*-band ones, since they are largely free of absorption effects and are more directly related to the stellar mass of the galaxy than optical luminosities. Nevertheless, this statement is correct only for galaxies with low and moderate SF activity. In emission-line galaxies with high star formation rate (SFR), such as blue compact dwarf (BCD) galaxies, the young, low mass-to-light (M/L) ratio stellar component may provide up to ~50% of the total *K* band emission (Noeske et al. , 2003). Additionally, in such systems the contribution of ionized gas to the total luminosity could be high (see e.g. Izotov et al. , 1997; Papaderos et al. , 1998, 2002), especially in the NIR range (see e.g. Vanzi et al. , 2000; Smith & Hancock , 2009), and should be taken into account.

Recently, studies of the $L - Z$ relation were extended to larger volumes by including moderate- and high-redshift galaxies (Kobulnicky & Zaritsky , 1999; Contini et al. , 2002; Maier et al. , 2004). Variations of the $L - Z$ relation with redshift can provide a means to study the galaxy evolution with look-back time (see, e.g., Kobulnicky et al. , 2003). It was established in this study that the slopes and zero points of the $L - Z$ relation evolve smoothly with redshift. Its large dispersion has been attributed to galaxy evolution effects. However, these results and their comparison with those for nearby galaxies should be considered with caution. The high-redshift samples are biased by different selection criteria and metallicity calibrations as compared to the local galaxies. They consist on average of more luminous and higher metallicity galaxies. Star-forming dwarf galaxies in the relatively high-redshift (up to $z \sim 1$) samples are rare because of their intrinsic faintness. Moreover, due to the weakness of the [O III]λ4363 emission line in the spectra of these galaxies, their abundance determinations are more uncertain and could lead to a large scatter in the $L - Z$ diagrams. This fact could be the reason for a larger scatter of high-redshift dwarf galaxies if the direct T_e-method is used instead of the empirical R_{23} one (e.g., Kakazu et al. , 2007).

In summary, it is difficult to obtain reliable metallicities over a large luminosity range in a homogeneous manner, i.e. employing a unique technique (e.g. the direct T_e-method), even for nearby galaxies. Therefore, different methods for abundance determination are applied for galaxies of different types. The direct method is mainly used for nearby low-metallicity galaxies, while various empirical methods are used for nearby high-metallicity galaxies and for almost all high-redshift galaxies. The variety of methods results in significant differences in the $L - Z$ relations obtained with the direct T_e-method and those based on strong emission line ratio calibrations, such as R_{23}, *P*-method, N2 and O3N2 methods. These differences were reported by many authors (e.g., Pilyugin et al. , 2004; Shi et al. , 2005; Hoyos et al. , 2005; Kakazu et al. , 2007).

Large surveys, such as the Two-Degree Field Galaxy Redshift Survey (2dFGRS) and Sloan Digital Sky Survey (SDSS), provide rich data sets for statistically improved studies of the $L - Z$ relation. For example, Lamareille et al. (2004) using more than 6000 spectra of SF galaxies at $z < 0.15$ from the 2dFGRS have obtained an $L-Z$ relation that is much steeper than that for nearby irregulars and spiral galaxies. Tremonti et al. (2004) studied the mass-metallicity ($M-Z$) relation for 53000 SF galaxies within $z \sim 0.2$ extracted from SDSS, using their stellar continuum and line fitting method. This method is applicable because the bulk of their emission-line galaxies show weak emission lines and strong stellar absorption features, and therefore the contribution of gaseous emission to the galaxy luminosity is low. The Tremonti et al. (2004) $M-Z$ relation is relatively steep but it flattens for massive galaxies at masses above 10^{10} $M_\odot$. On the contrary, Melbourne & Salzer (2002) using 519 emission-line galaxies from the KPNO International Spectroscopic Survey (KISS) found that the slope of the $L - Z$ relation for luminous galaxies is steeper than that for dwarf galaxies. Nevertheless, Pilyugin et al. (2004) have compared the $L - Z$ relation based on more than 1000 published spectra of H II regions in spiral galaxies to that for irregular galaxies. They found that the slope of the relation for spirals is slightly shallower than the one for irregular galaxies. Furthermore, using 72 star-forming galaxies, Shi et al. (2005) have also shown that the slope of the $L - Z$ relation for luminous galaxies is slightly shallower than that for dwarf galaxies.

Is the slope of the $L - Z$ relation invariant for galaxies of different type, such as local dwarf and spiral galaxies and high-redshift galaxies? If differences in the $L - Z$ relations for intermediate- and high-redshift and local ones are present, they may yield important constraints on the Star Formation History (SFH) of galaxies. For this, an as accurate as possible $L-Z$ relation, based on homogeneous high-quality photometric and spectroscopic data is required for galaxies that covers a large range in metallicity and luminosity. In particular, probing the slope of the $L - Z$ relation in its low-metallicity end, i.e. in the range expected for unevolved low-mass galaxies in the faraway universe, is much needed. For this purpose, in this paper we focus our study on the lowest-metallicity galaxy candidates selected from large spectroscopic surveys, using deep follow-up spectroscopic observations.

Specifically, the objective of the work is to study the $L-Z$ relation for a large uniform sample of emission-line galaxies in the local Universe for which the element abundances are obtained with high precision. The main feature of our sample is that it is one of the richest currently available at the low-metallicity end. For the galaxy selection we used different surveys such as 2dFGRS, SDSS and others. Most of our sample galaxies currently undergo strong episodes of star formation (SF).

We performed 3.6m ESO spectroscopic observations of a sample of 38 H II regions in 28 emission-line galaxies and 8.2m VLT spectroscopic observations of a sample of 28 H II regions in 16 emission-line galaxies. We supplement our new data with our previous data collected from the MMT observations (Izotov & Thuan , 2007), and from the 3.6m ESO observations (Guseva et al. , 2007; Papaderos et al. , 2008) of the low-metallicity emission-line galaxies selected from the SDSS, with the sample used by Izotov & Thuan (2004) to study the helium abundance in low-metallicity BCDs (henceforth referred

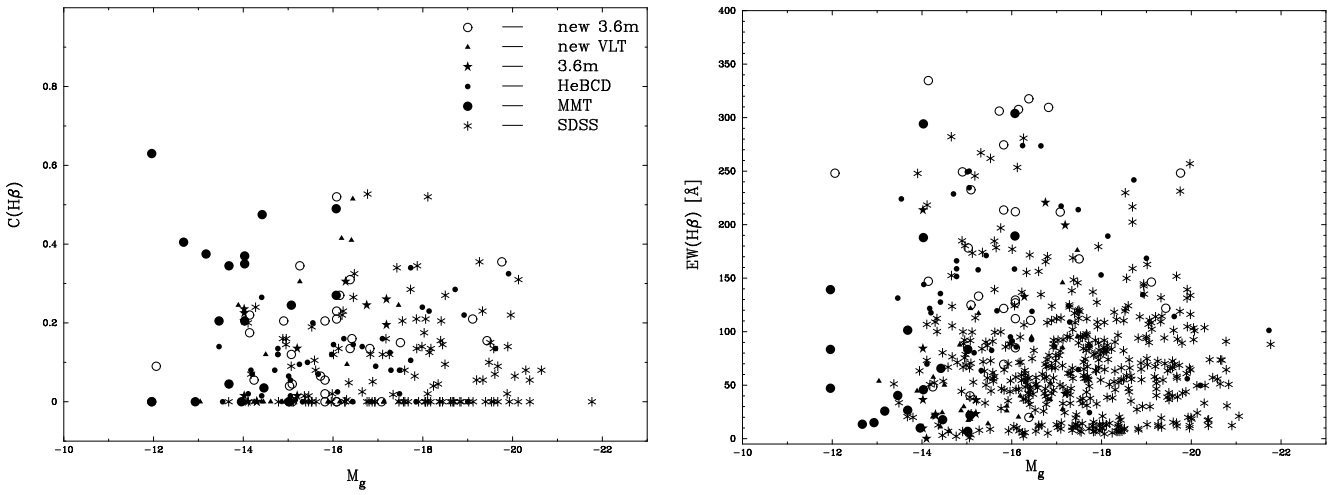

Fig. 3. The reddening parameter $C(\mathrm{H}\beta)$ obtained from the observed Balmer decrement (left) and the logarithm of the Hβ equivalent width (in Å) (right) as a function of the absolute magnitude M_g in the SDSS g-band. Oxygen abundances are derived mainly with the T_e-method. Additionally, only high-quality SDSS spectra with the non-detected [O III]λ4363 emission line are included for which oxygen abundances are derived with the semiempirical method (Izotov & Thuan , 2007). New 3.6m ESO telescope and VLT data are shown by open circles and by stars, respectively. The additional sample of the metal-poor galaxies collected from previous 3.6m ESO observations (Guseva et al. , 2007) are shown by filled triangles. Filled circles denote the data from the HeBCD sample collected by Izotov et al. (2004b) and Izotov & Thuan (2004). The MMT data from Izotov & Thuan (2007) are shown by large filled circles. The comparison SDSS sample is represented by asterisks in which are excluded the H II regions in nearby spiral galaxies, faint galaxies with $m_g > 18$, the nearest galaxies with redshift $z < 0.004$ and all galaxies with $\sigma I(4363)/I(4363) > 0.25$, resulting in the SDSS sample of 443 objects.

to as the HeBCD sample) and with the MMT sample used by Thuan & Izotov (2005) to study high-ionization emission lines in low-metallicity BCDs. Our MMT, 3.6m ESO and HeBCD low-metallicity galaxies were selected from different surveys (a more complete description of the MMT, 3.6m ESO and HeBCD subsamples can be found in Izotov & Thuan , 2007; Guseva et al. , 2007; Papaderos et al. , 2008; Izotov & Thuan , 2004). During past years we selected from the SDSS and performed follow-up spectroscopic observations with large telescopes of (i) BCDs with strong ongoing SF, i.e. galaxies with high EW(Hβ), blue colours, high ionisation parameter, and (ii) low-metallicity galaxies in a relatively quiescent phase of SF, i.e. galaxies with low EW(Hβ), low ionisation parameter or older starburst age. For this, we selected galaxies with weak or not detected [O III]λ4363 emission line and with [O III]λ4959/H$\beta \lesssim 1$ and [N II]λ6583/H$\beta \lesssim 0.05$ (Izotov et al. , 2006b; Izotov & Thuan , 2007).

SDSS is an excellent source of both photometric and spectroscopic data for more than one million galaxies in its Data Release 7 (DR7) (Abazajian et al. , 2009). Despite that, our stringent selection criteria resulted in a very small sample of extremely metal-deficient emission-line galaxies with reliable abundance determinations. This sample is supplemented for the purpose of comparison by a sample of ∼ 9000 SDSS emission-line galaxies (SDSS sample) over a larger range of metallicities. The oxygen abundances for the galaxies from the SDSS sample are obtained using the direct T_e-method. In addition, only high-quality spectra of SDSS galaxies with the non-detected [O III]λ4363 emission line are included, for which oxygen abundances are derived by a semiempirical method (Izotov & Thuan , 2007).

Thus, we construct a large homogeneous sample with uniform selection criteria, uniform data reduction methods, and uniform techniques for the element abundance determinations. The apparent g magnitudes for our entire data set are taken from the SDSS. They were used to derive absolute g magnitudes which were corrected for the Galactic extinction and Virgo cluster infall, except for the comparison SDSS sample galaxies. For the latter galaxies the absolute magnitude was derived from the observed redshift, adopting a Hubble constant of $H_0 = 75$ km s^{-1} Mpc^{-1}.

The paper is organized as follows. Observations and data reduction are described in Sect. 2. Physical conditions and element abundances in the galaxies from the new observations are presented in Sect. 3. We discuss the properties of the $L - Z$ relation in Sect. 4 and summarise our conclusions in Sect. 5.

2. Observations and data reduction

The new spectra of the 3.6m ESO sample were obtained on 14 - 16 September, 2007 with the spectrograph EFOSC2. The grism Gr#7 and a long slit with the width of 1.″2 were used yielding a wavelength coverage of $\lambda\lambda$3400–5200. The long slit was centered on the brightest part of each galaxy and simultaneously on another H II regions, whenever present. The name of each galaxy with its different H II regions, the coordinates R.A., Dec. (J2000.0), date of observation, exposure time, number of exposures for each observation, average airmass and seeing are given in Table 1. All spectra were obtained at low airmass or with the slit oriented along the parallactic angle, so no corrections for atmospheric refraction have been applied.

The new VLT spectra were obtained during several runs in October - December, 2006 and January, 2007 with the spectrograph FORS2 mounted at the ESO VLT UT2. The observing conditions were photometric during the nights with seeing < 1.″5. Several observations were performed under excellent seeing conditions (< 0.″8). The grisms 600B ($\lambda\lambda$∼3400–6200) and 600RI and filter GG435 ($\lambda\lambda$∼5400–8620) for the blue and red parts of the spectrum, respectively, were used. A 1″×360″ long slit was centered on the brightest H II regions of each galaxy. In

Table 2, the same parameters as in Table 1 are given for the VLT observations. Note that for each galaxy the first and the second lines are related to the observations in the blue and red ranges, respectively. Again, as for the EFOSC2 spectra, the observations were obtained at low airmass, and no corrections for atmospheric refraction were applied.

The data were reduced with the IRAF[1] software package. This included bias–subtraction, flat–field correction, cosmic-ray removal, wavelength calibration, night sky background subtraction, correction for atmospheric extinction and absolute flux calibration of the two–dimensional spectrum. The spectra were also corrected for interstellar extinction using the reddening curve of Whitford (1958). One-dimensional spectra of one or several H II regions in each galaxy were extracted from two-dimensional observed spectra. The flux- and redshift-calibrated one–dimensional EFOSC2 3.6m spectra of the H II regions are shown in Fig. 1 for all galaxies given in Table 1. One-dimensional VLT spectra are shown in Fig. 2 for 28 objects listed in Table 2. For VLT spectra of the four background galaxies and H II region No.2 in the galaxy J2354-0004 without a detectable [O III]λ4363Å emission line, no abundance determination has been done.

Emission-line fluxes were measured using Gaussian profile fitting. The errors of the line fluxes were calculated from the photon statistics in the non-flux-calibrated spectra. They have been propagated in the calculations of the elemental abundance errors. The quality of the VLT data reduction could be verified by a comparison of He I λ5876 emission line fluxes measured in the blue and red spectra of the same object. We found that the fluxes of the He I λ5876 emission line in spectra of bright objects differ by no more than 1-2% indicating an accuracy in the flux calibration at the same level. For faint objects the difference between the flux of the He I λ5876 emission line in the blue and red spectra is higher, $\sim$5 – 10%, and is comparable to the statistical errors listed in Table 4.

The extinction coefficient $C(\mathrm{H}\beta)$ and equivalent widths of the hydrogen absorption lines EW(abs) are calculated simultaneously, minimizing the deviations of corrected fluxes $I(\lambda)/I(\mathrm{H}\beta)$ of all hydrogen Balmer lines from their theoretical recombination values as

$$\frac{I(\lambda)}{I(\mathrm{H}\beta)} = \frac{F(\lambda)}{F(\mathrm{H}\beta)} \frac{EW(\lambda)+|EW(abs)|}{EW(\lambda)} \frac{EW(\mathrm{H}\beta)}{EW(\mathrm{H}\beta)+|EW(abs)|} \times 10^{C(\mathrm{H}\beta)f(\lambda)}.$$

Here $f(\lambda)$ is the reddening function normalized to the value at the wavelength of the Hβ line, $F(\lambda)/F(\mathrm{H}\beta)$ are the observed hydrogen Balmer emission line fluxes relative to that of Hβ, EW(λ) and EW(Hβ) the equivalent widths of emission lines, and EW(abs) the equivalent widths of hydrogen absorption lines which we assumed to be the same for all hydrogen lines. For $f(\lambda)$ we adopted the reddening law by Whitford (1958). The extinction-corrected fluxes of emission lines other than hydrogen ones are derived from equation

$$\frac{I(\lambda)}{I(\mathrm{H}\beta)} = \frac{F(\lambda)}{F(\mathrm{H}\beta)} \times 10^{C(\mathrm{H}\beta)f(\lambda)}.$$

The extinction-corrected emission line fluxes $I(\lambda)$ relative to the Hβ fluxes multiplied by 100, the extinction coefficients $C(\mathrm{H}\beta)$, the equivalent widths EW(Hβ), the observed Hβ fluxes $F(\mathrm{H}\beta)$ (in units 10^{-16} erg s^{-1} cm^{-2}), and the equivalent widths of the hydrogen absorption lines are listed in Table 3 (3.6m ESO observations) and in Table 4 (VLT observations). $C(\mathrm{H}\beta)$ and EW(abs) are set to zero in Tables 3 and 4 if we do not have enough observational data or their values are negative.

[1] IRAF is the Image Reduction and Analysis Facility distributed by the National Optical Astronomy Observatory, which is operated by the Association of Universities for Research in Astronomy (AURA) under cooperative agreement with the National Science Foundation (NSF).

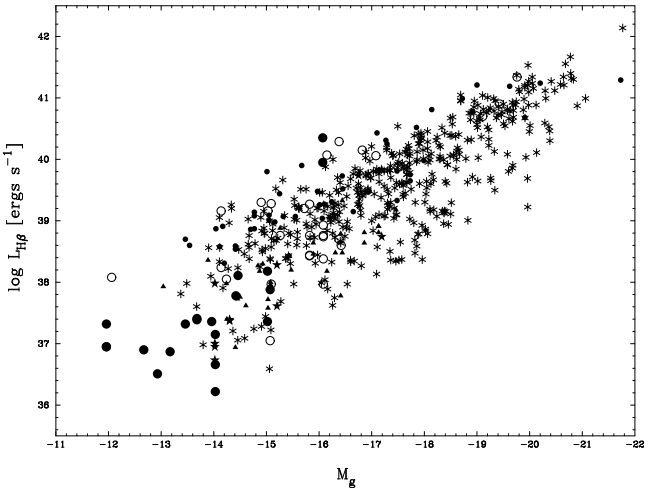

Fig. 4. The logarithm of the Hβ line luminosity (in ergs s^{-1}) vs absolute magnitude. The same samples and symbols as in Fig 3 are used.

3. Physical conditions and element abundances

The electron temperature T_e, the ionic and total heavy element abundances were derived following Izotov et al. (2006a). In particular, for the ions O^{2+}, Ne^{2+} and Ar^{3+} we adopt the temperature T_e(O III) directly derived from the [O III] λ4363/(λ4959 + λ5007) emission-line ratio. For T_e(O II) and T_e(S III) we use the relation between the electron temperatures T_e(O III) and the temperatures characteristic for ions O^+ and S^{2+} obtained by Izotov et al. (2006a) from the H II photoionization models based on recent stellar atmosphere models and improved atomic data (Stasińska & Izotov , 2003).

We use T_e(O II) for the calculation of O^+, N^+, S^+ and Fe^{2+} abundances and T_e(S III) for the calculation of S^{2+}, Cl^{2+} and Ar^{2+} abundances. The electron number densities for some H II regions were obtained from the [S II] λ6717/λ6731 emission line ratio. These lines were not observed or not measured in the remaining H II regions. For the abundance determination in those H II regions we adopt N_e = 10 cm^{-3}. The precise value of the electron number density makes little difference in the derived abundances since in the low-density limit which holds for the H II regions considered here, the element abundances do not depend sensitively on N_e. The electron temperatures T_e(O III), T_e(O II), the ionization correction factors (ICFs), the ionic and total O and Ne abundances are given in Table 5 for 3.6m observations. The electron temperatures T_e(O III), T_e(O II), T_e(S III), electron number density N_e([S II]), the ionization correction factors (ICFs), the ionic and total O, N, Ne, S, Cl, Ar and Fe abundances are given in Table 6 for VLT observations.

The oxygen abundances 12 + log O/H in 61 H II regions out of 66 obtained from the new 3.6m ESO and VLT observations range from 7.05 to 8.22. Among them, 27 H II regions with 12 + log O/H < 7.6 are found, including 10 H II regions with 12 + log O/H < 7.3. The combined sample consisting of the

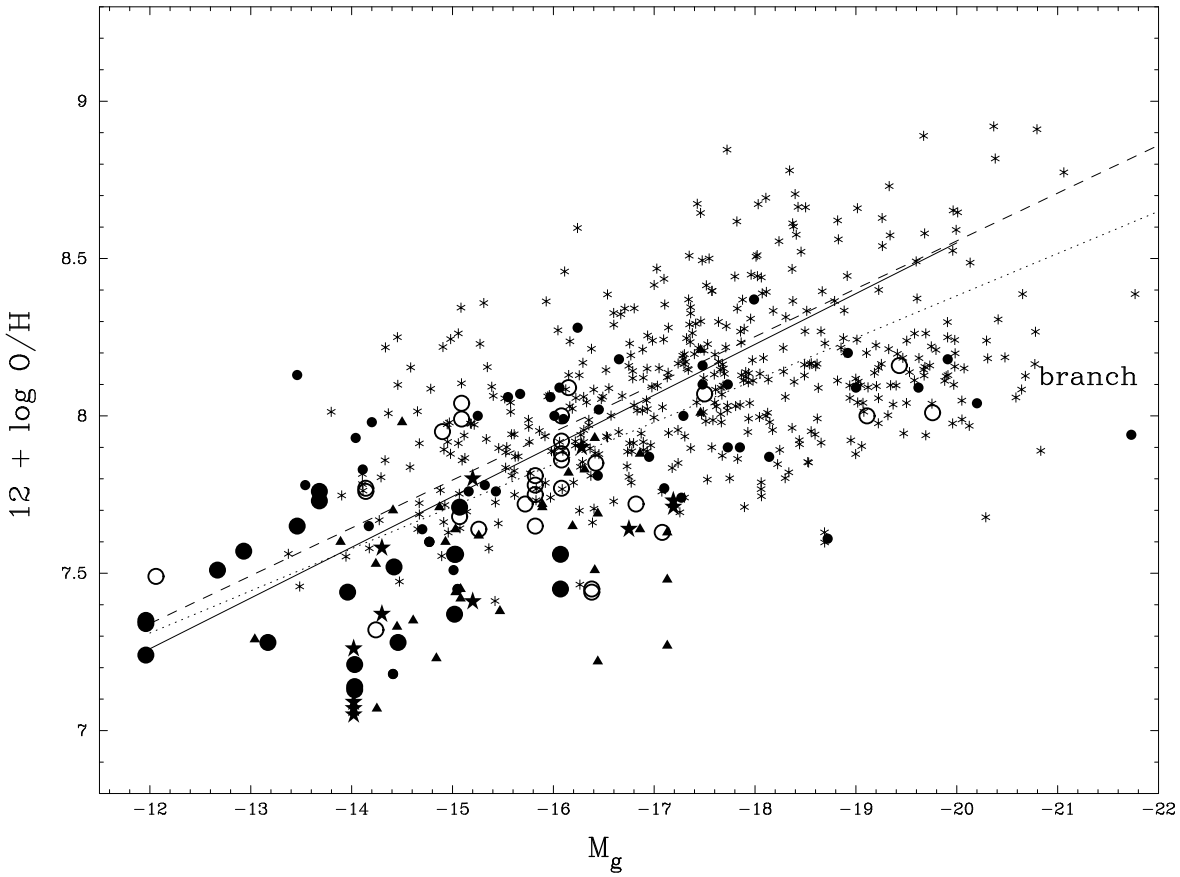

Fig. 5. Oxygen abundance vs absolute magnitude for a large galaxy sample. The same samples and symbols as in Fig 3 are used. The region denoted as a "branch" is populated mainly by the galaxies with relatively high redshifts ($z > 0.02$) and oxygen abundances derived by the T_e-method. The dotted line is a mean least-squares fit to all our data, while the solid line is a mean least-squares fit to our data excluding "branch" galaxies with $M_g < -18.4$ and oxygen abundances in the range 8.0–8.3. The dashed line is a mean least-squares fit to the local dwarf irregular galaxies by Skillman et al. (1989).

new observations, 43 BCDs from the HeBCD sample, 30 galaxies from our previous 3.6m ESO observations and 20 galaxies from the MMT observations yields a data set of 154 H II regions. For comparison, we also use ∼9000 SDSS emission-line galaxies with the [O III] λ4363 emission line detected at least at the 1σ level, allowing abundance determination by the direct T_e-method. In addition, SDSS galaxies with high-quality spectra where the [O III]λ4363 emission line was not detected are used. In the latter case, the oxygen abundances were derived by the semiempirical method. SDSS galaxies from the comparison sample mostly populate the high-metallicity, high-luminosity ranges, as compared to the galaxies from our combined sample of low-metallicity emission-line galaxies (Figs. 5 - 7). The considered galaxies span two dex in gas-phase oxygen abundance, from 12 + log O/H ∼ 7.0 through ∼ 9.0.

We use SDSS *g* magnitudes for the determination of the absolute magnitude M_g of all galaxies from our samples, while usually *B* magnitudes and M_B are considered in the literature. However, Papaderos et al. (2008) have shown that for regions with ongoing bursts of star formation, which is the case for our sample galaxies, the *B–g* colour index is of the order of 0.1 mag only and <0.3 mag during the first few Gyrs of galactic evolution. Therefore, we do not transform M_g to M_B and directly compare M_g's for the galaxies from our samples with M_B's for the galaxies available from the literature. The use of the SDSS *g*-band photometry for all our samples allows us to investigate the $L-Z$ relation over the M_g range from –21 mag to the faintest magnitude of ∼ –12 mag at the low-metallicity end.

4. Results

4.1. Luminosity-metallicity relation

In order to illustrate the main properties of our sample we plot (a) the reddening parameter $C(H\beta)$ obtained from the Balmer decrement and (b) the logarithm of the Hβ equivalent width (Fig. 3) and the logarithm of the Hβ line luminosity (in erg s^{-1}) (Fig. 4) as a function of absolute magnitude M_g. The new 3.6m telescope and VLT data are shown by open circles and stars, respectively. The metal-poor galaxies collected from previous 3.6m ESO observations are shown by filled triangles (Guseva et al. , 2007; Papaderos et al. , 2008). Filled circles denote the data from the HeBCD sample collected by Izotov et al. (2004a) and Izotov & Thuan (2004). The MMT data (Izotov & Thuan , 2007) are shown by large filled circles. The comparison SDSS sample is represented by asterisks. From the latter sample H II regions in nearby spiral galaxies are excluded, as are faint SDSS galaxies with $m_g > 18$, the nearest SDSS galaxies with the redshift $z < 0.004$ and all SDSS galaxies with $\sigma[I(4363)]/I(4363) > 0.25$, totaling 443 SDSS galaxies from the comparison sample.

Our sample does not show any trend with absolute magnitude of either $C(H\beta)$ or EW(Hβ), contrary to what was obtained

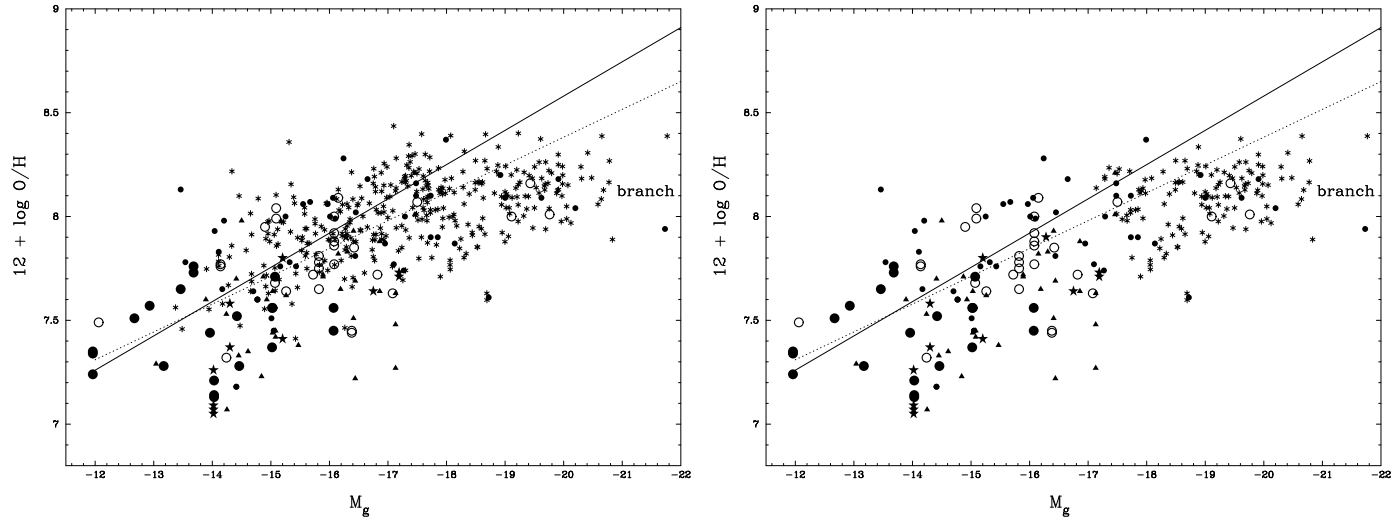

Fig. 6. The same as in Fig 5 but (left) only SDSS galaxies with oxygen abundances derived with the T_e-method and (right) only relatively high-redshift galaxies with z> 0.02. The dotted line is a mean least-squares fit to all our data, while the solid line is a mean least-squares fit to our data excluding "branch" galaxies.

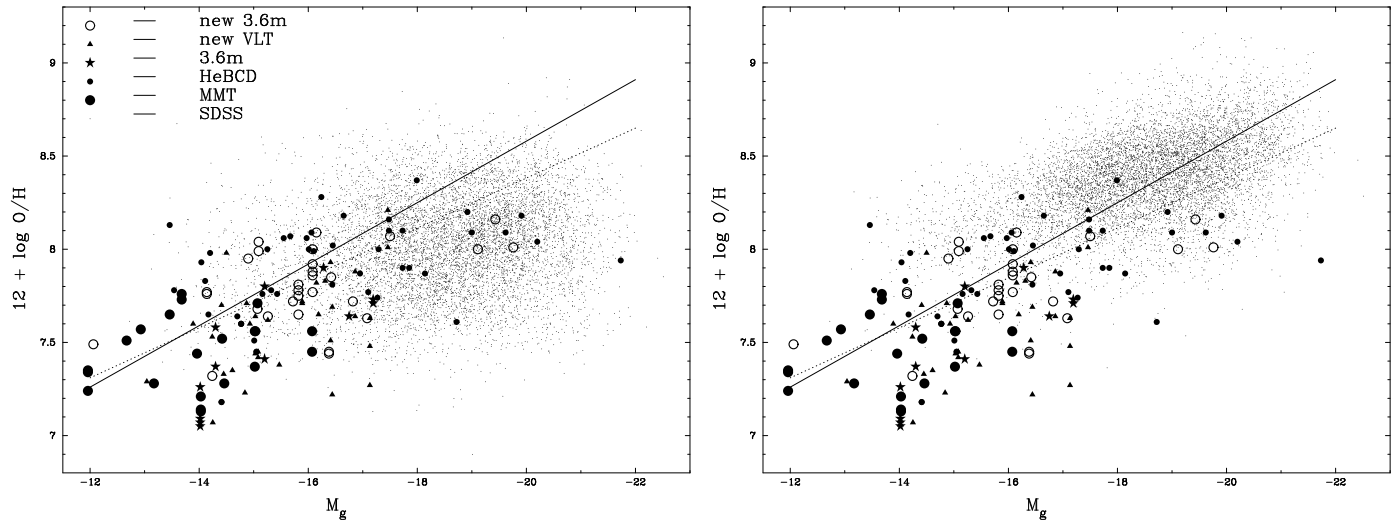

Fig. 7. Oxygen abundance vs absolute magnitude. H II regions in spiral galaxies and the nearest SDSS galaxies with redshift $z < 0.004$ are excluded from the SDSS sample while faint galaxies with $m_g > 18$ are included, resulting in an SDSS sample of 7964 objects. Symbols are the same as in Fig. 3 except for SDSS galaxies which are shown by dots. In the left panel the oxygen abundances 12 +logO/H for SDSS galaxies are obtained with the T_e-method. In the right panel 12 +logO/H for SDSS galaxies is derived with the semiempirical method. The dotted line is a mean least-squares fit to all our data from Fig. 5, while the solid line is a mean least-squares fit to the same data excluding "branch" galaxies.

by Salzer et al. (2005) for the KISS sample. The extinction in our sample galaxies is low. Only a few galaxies have $C(H\beta) > 0.4$. The range of EW(Hβ) ~ 0 – 300 Å for the galaxies from our sample is similar to that for the KISS sample (Salzer et al. , 2005) but it is higher than that for the high-redshift galaxies of Kobulnicky et al. (2003) where EW(Hβ) ≤ 60 Å.

The logarithm of the Hβ luminosity log L(Hβ) of our galaxies ranges from 36 to 42 (Fig. 4). For comparison, the galaxies from the KISS sample by Salzer et al. (2005) and intermediate-redshift galaxies by Kobulnicky et al. (2003) have log L(Hβ) ~ 39 – 43 and 39 – 42, respectively, i.e. low-luminosity galaxies are lacking.

In Fig. 5 we show the oxygen abundance - absolute magnitude M_g relation for the galaxies with oxygen abundances calculated mainly with the T_e-method. In this Figure, the same samples and symbols as in Fig 3 are used. The region denoted as "branch" is populated mainly by galaxies with relatively high redshifts ($z > 0.02$) and oxygen abundances derived by the T_e-method. Note that selection effects could be present for "branch" high-redshift galaxies which are predominantly distant spirals. In these galaxies we select mainly low metallicity H II regions with a detectable [O III]λ4363 line while the abundance gradient is present in spirals. The dotted line is a mean least-squares fit to all our data and the solid line is a mean least-squares fit to our data excluding "branch" galaxies with $M_g < -18.4$ and systems with an oxygen abundance in the range 8.0 – 8.3. The dashed line is a mean least-squares fit to the local dwarf irregular galaxies by Skillman et al. (1989). Our sample (including the SDSS subsample) shows the familiar trend of increasing metal-

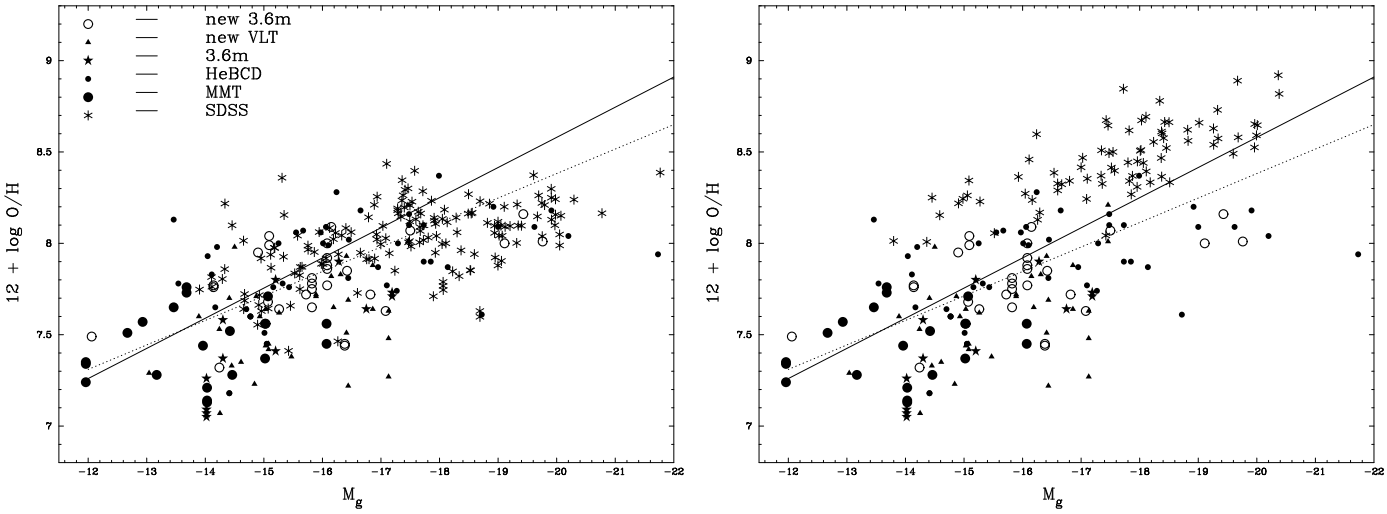

Fig. 8. The same as in Fig. 5 but only SDSS galaxies with EW(Hβ) > 80Å (left panel) and with EW(Hβ) < 20Å (right panel). The dotted line is a mean least-squares fit to all our data from Fig. 5, while the solid line is a mean least-squares fit to the same data excluding "branch" galaxies. For the SDSS galaxies with EW(Hβ) > 80Å the oxygen abundances are ∼ 0.4 dex lower than the ones for the galaxies with EW(Hβ) < 20Å. The galaxies with the lowest metallicities could be found more easily among the H II regions with high EW(Hβ).

licity with increasing luminosity. A linear least square fit to all data yields the relation

$$12 + \log(\mathrm{O/H}) = (5.706 \pm 0.199) - (0.134 \pm 0.012)\mathrm{M}_g \qquad (1)$$

(dotted line in Fig. 5). Excluding "branch" galaxies we obtain the relation

$$12 + \log(\mathrm{O/H}) = (5.076 \pm 0.320) - (0.174 \pm 0.200)\mathrm{M}_g \qquad (2)$$

(solid line in Fig. 5). We note that the Skillman et al. and Richer & McCall fits do not extend over the metallicity range of the present data. Therefore, we extrapolate the former fit in Fig. 5 (dashed line) to higher metallicities. Skillman's and our fits are obviosuly very similar. The slopes of our $L - Z$ relation of 0.134 (0.174) are very close to the slope of 0.153 by Skillman et al. (1989) and to the slope of 0.147 by Richer & McCall (1995).

Our sample is well populated in the low-luminosity range, while less than 10 galaxies from the KISS sample (Salzer et al. , 2005) which were used for the study of the $L - Z$ relation are fainter than M_B = –15, and none of them has an oxygen abundance less than 7.6. Our sample, excluding the SDSS subsample, has a lower dispersion around the dotted line compared to all our data and shows a shift to lower metallicities or/and higher luminosities. This likely can be attributed to our selection criteria which are optimized for the search for very metal-poor emission-line galaxies. Additionally, our sample galaxies display significant to strong ongoing SF giving rise to a large contribution from young stars and ionized gas to the total light of the galaxy. Papaderos et al. (1996, see also Papaderos et al. (2002)), using surface brightness profile decomposition to separate the star-forming component from the underlying host galaxy of BCDs, found that SF regions provide on average 50% of the total B-band emission within the 25 B mag/□″ isophote, with several examples of more intense starbursts whose flux contribution exceeds 70%. As a result, a shift of BCDs by a ΔM ∼–0.75 mag with respect to the relatively quiescent dIrr population is to be expected in Fig. 5 (see also Fig. 9). A similar offset to lower metallicities or/and higher luminosities has been found by Kakazu et al. (2007) for their intermediate-redshift low-metallicity emission-line galaxies with strong SF activity. The mass estimate of the galaxy is less sensitive to the presence of star-forming regions as compared to its luminosity. This was demonstrated by Ellison et al. (2008) who found that galaxies in close pairs show enhanced SF activity as compared to a control sample of isolated galaxies. At the same time galaxies in close pairs show a smaller offset in the mass-metallicity relation as compared to the luminosity-metallicity relation. Thus, the offset in Fig. 5 indicates that both higher luminosities and lower metallicities may contribute to the shift in the luminosity-metallicity diagram of our sample galaxies relative to more quiescent dIrrs.

In Fig. 6 we demonstrate that the region of "branch" galaxies is populated mainly by relatively high-redshift systems. The sample is the same as in Fig. 5 but in the left panel only SDSS galaxies with oxygen abundances derived with the T_e-method are shown and in the right panel only relatively high-redshift galaxies with $z > 0.02$ are selected.

The location of the galaxies on the luminosity-metallicity diagram is also sensitive to the method used for the abundance determination. In order to illustrate its effect on the observed $L - Z$ relation, we compare in Fig. 7 the oxygen abundance of SDSS sample galaxies (dots) obtained with the direct T_e-method (left panel) and with the semiempirical strong-line method (right panel). The abundances for other galaxies in Fig. 7 are derived with the T_e-method. In this Figure we show the larger control sample of the SDSS (N=7964) as compared to Fig. 5. Only H II regions in nearby spiral galaxies and from the nearest SDSS galaxies with redshifts $z < 0.004$ were excluded from the ∼ 9000 SDSS sources while faint galaxies with $m_g > 18$ are included. Symbols in Fig. 7 are the same as in Fig. 3 except for SDSS galaxies which are shown by dots. The dotted line is a mean least-squares fit to all our data from Fig. 5, while the solid line is a mean least-squares fit to the same data excluding "branch" galaxies.

It can be seen from Fig. 7 that the oxygen abundance of a given galaxy obtained by different methods could differ by ∼0.3–0.5 dex, especially for luminous galaxies. This figure illustrates clearly above 12 + log O/H ∼ 8.5 and M_g < –19 - –20 significant discrepancies between oxygen abundances obtained

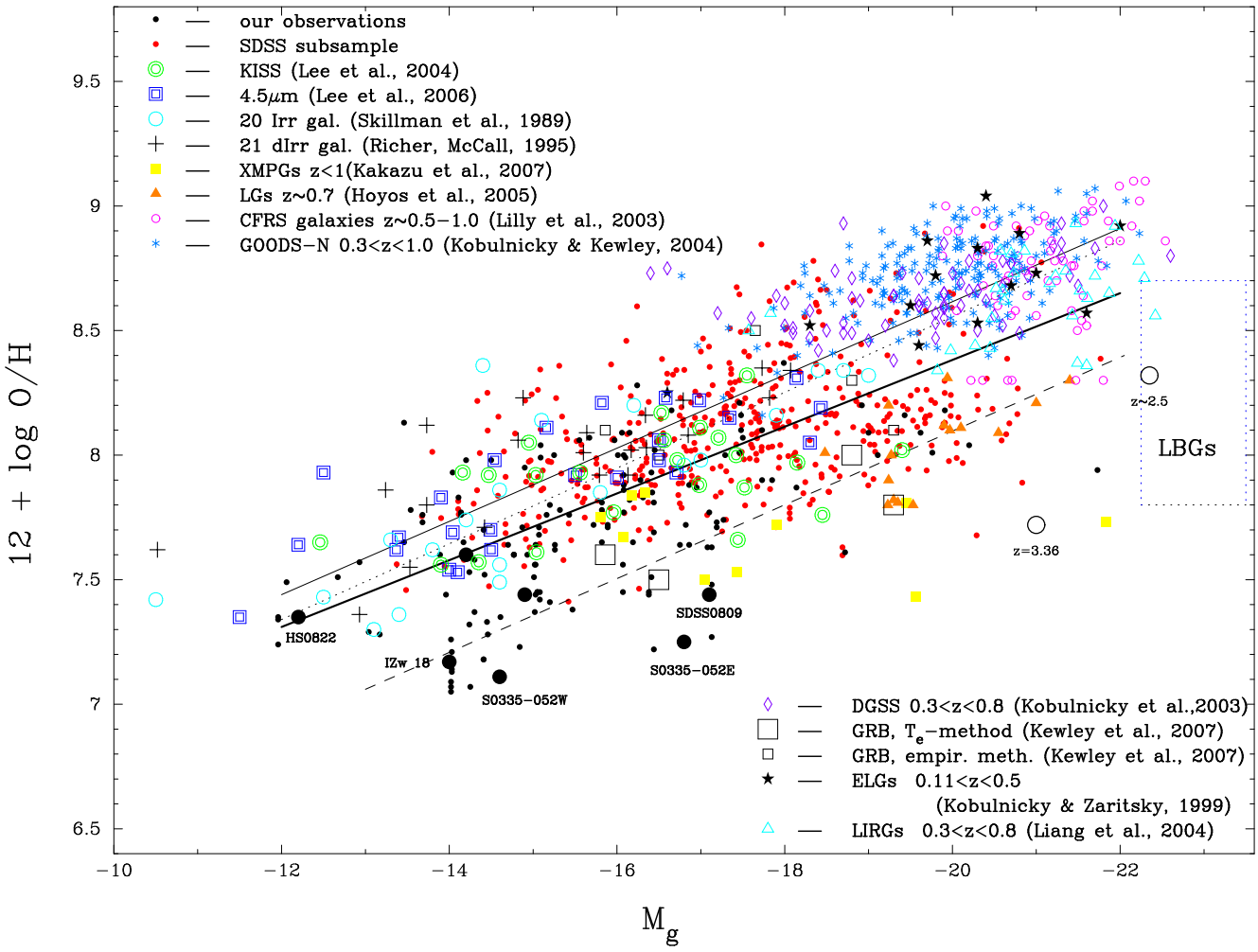

Fig. 9. Oxygen abundance vs absolute magnitude for the same galaxies as in Fig. 5 but all our galaxies including the SDSS sample are shown by small filled circles. Additionally, some well known metal-poor galaxies, intermediate- and high-redshift galaxies are shown by symbols as labelled in the figure. The position of the Lyman break galaxies (LBGs) by Pettini et al. (2001) is indicated by the dotted line rectangle. The thick solid line is a mean least-squares fit to all our data. The thin solid line is a least-squares fit to the data by Richer & McCall (1995) while the dotted line is a mean least-squares fit to the data by Skillman et al. (1989). The dashed line is the luminosity-metallicity relation for local metal-poor BCDs obtained by Kunth & Östlin (2000).

from the T_e-method and empirical methods. Stasińska (2002) emphasized that, at high metallicity, the T_e derived from [O III] λ4363 would largely overestimate the temperature of the O^{++} zone (and largely underestimate the metallicity) because cooling is dominated by the [O III] λ52 μm and [O III] λ88 μm lines. At the same time Pilyugin et al. (2007) demonstrated that there is an observational limit of the highest possible metallicities near 12 + log O/H ∼ 8.95. This maximum value was determined in the centers of the most luminous ($-22.3 \lesssim M_B \lesssim -20.3$) galaxies using the semiempirical ff-method (Pilyugin et al. , 2006). Thus, although the main mechanisms determining the electron temperature in H II nebulae have been known for a long time, there are still important unsolved problems.

The contribution of star-forming regions to the light of the galaxy can be quantified by the equivalent width EW(Hβ) of the Hβ emission line which in turn depends on the age of the burst of star formation. In Fig. 8 we show the same samples as in Fig. 5 except for the SDSS galaxies now being split into two subsamples. In the left panel only those with high equivalent widths EW(Hβ) > 80Å are shown while in the right panel only SDSS galaxies with low equivalent widths EW(Hβ) < 20Å are plotted. The dotted line in the left and right panels is a mean least-squares fit to all our data shown in Fig. 5, while the solid line is a mean least-squares fit to the same data excluding "branch" galaxies. There is a clear difference between the two subsamples of the SDSS galaxies by ∼ 0.4 dex in oxygen abundance or, equivalently, by ∼ 3 mag in absolute magnitude. SDSS galaxies with EW(Hβ) > 80Å nicely follow the relation for our dwarf low-metallicity emission-line galaxies shown as reference objects by filled and open circles, stars, filled triangles and large filled circles. On the other hand, the SDSS galaxies with EW(Hβ) < 20Å are located systematically above the low-metallicity galaxies. We propose two possible explanations for such a difference between the two subsamples of SDSS galaxies: 1) the emission of the SDSS galaxies with high EW(Hβ) is dominated by star-forming regions, therefore they have higher luminosities compared to galaxies in a relatively quiescent stage; 2) SDSS galaxies with low EW(Hβ) are the ones with higher astration level, therefore they are more chemically evolved systems with higher oxygen abundances. Perhaps both of these explanations are tenable, accounting for the observed differences between SDSS galaxies with high and low EW(Hβ).

Thus, the lowest-metallicity SDSS galaxies are found predominantly among galaxies with high EW(Hβ). On the other hand, no extremely low-metallicity SDSS galaxies are found among systems with EW(Hβ) < 20Å. Thus, mixing of the SDSS galaxies with EW(Hβ) < 20Å and > 80Å results in a significant increase of the dispersion of the luminosity-metallicity diagram.

The redshift of the galaxy could also play a role. In Fig. 5 the bulk of the galaxies with 12+log(O/H)=8.0 – 8.3 and absolute magnitudes between –19 and –21 mag (denoted as "branch" galaxies) is represented by higher-redshift systems as compared to other galaxies from the SDSS and a correction for redshift is required. Since "branch" galaxies are blue, a correction for redshift for systems with weak emission lines would increase their brightness by ~ 0.1 - 0.3 mag. This will not be enough to remove the offset between "branch" galaxies and lower-redshift galaxies in Fig. 5. The situation is more complicated for "branch" galaxies with strong emission lines since their effect on the apparent magnitudes of a galaxy in standard passbands will significantly depend on redshift (see e.g. Zackrisson et al. , 2008). Because of these reasons, we decided not to take into account corrections for redshift.

4.2. Comparison of our sample with other data

In Fig. 9 we compare our $L - Z$ relation with other published data for galaxies of different types. In this Figure, all of our galaxies from Fig. 5, including those from the comparison SDSS sample, are shown by small filled circles. Some well known metal-poor galaxies are depicted by large filled circles and are labelled. Their absolute magnitudes M_B are taken from Kewley et al. (2007). For comparison, 23 KISS emission-line galaxies by Lee et al. (2004) are displayed with large open double circles. The abundances for these galaxies are derived with the T_e-method, the *B*-band magnitudes are from Salzer et al. (1989) and Gil de Paz et al. (2003). With open double squares we show 25 nearby dIrrs with the 4.5μm *Spitzer* luminosities and compiled O/H abundances derived with the T_e-method (Lee et al. , 2006). With large open circles and large crosses we respectively show 20 irregular galaxies from Skillman et al. (1989) and 21 dwarf irregular galaxies from Richer & McCall (1995) for which oxygen abundances are obtained mainly with the R_{23} empirical method, and for a few objects only with the T_e-method. The thick solid line is a mean least-squares fit to all our data. The thin solid line is a least-squares fit to the data by Richer & McCall (1995) while the dotted line is a mean least-squares fit to the data by Skillman et al. (1989). The dashed line is the luminosity-metallicity relation for local metal-poor BCDs obtained by Kunth & Östlin (2000).

Data for intermediate- and high-redshift galaxies are also shown. The most distant (z < 1) extremely metal-poor galaxies (XMPGs) (Kakazu et al. , 2007) with the oxygen abundances derived with the empirical method are shown with filled squares, while relatively metal-poor luminous galaxies at z ~ 0.7 (Hoyos et al. , 2005) (O/H derived with the T_e-method) with filled triangles. The remaining samples in Fig. 9 are the following: a) the large open circles correspond to the z = 3.36 lensed galaxy (Villar-Martín et al. , 2004) and to the average position of luminous Lyman-break galaxies at redshifts z ~ 2.5 (Kobulnicky & Koo , 2000) (O/H derived with the R_{23} method); b) small open circles stand for 66 Canada-France Redshift Survey (CFRS) galaxies by Lilly et al. (2003) in the redshift range of ~ 0.5 – 1.0 (O/H derived with the R_{23} empirical method); c) asterisks are for 204 GOODS-N (Great Observatories Origins Deep Survey - North) emission-line galaxies in the range of redshifts 0.3 < z < 1.0 (Kobulnicky & Kewley , 2004) (O/H is derived with the R_{23} empirical method); d) small open rombs indicate 64 emission-line field galaxies from the Deep Extragalactic Evolutionary Probe Groth Strip Survey (DGSS) in the redshift range of ~ 0.3 – 0.8 (Kobulnicky et al. , 2003) (O/H derived with the R_{23} empirical method); e) open squares are for the gamma-ray burst (GRB) hosts by Kewley et al. (2007). Small open squares are for galaxies with O/H derived with the empirical method (Kewley & Dopita , 2002) and large open squares for the galaxies with O/H derived with the T_e-method (Kewley et al. , 2007); f) filled stars denote the 14 star-forming emission-line galaxies at intermediate redshifts (0.11 < z < 0.5) by Kobulnicky & Zaritsky (1999) (O/H derived with the empirical R_{23} method); g) open filled triangles are for 29 distant 15μm-selected luminous infrared galaxies (LIRGs) at z ~ 0.3 – 0.8 taken from the sample of Liang et al. (2004) (O/H derived with the empirical method); and, finally, h) the large dotted rectangle depicts the position of Lyman break galaxies (LBGs, Pettini et al. , 2001) on the $L - Z$ diagram.

The location of our galaxies on the luminosity-metallicity diagram is similar to that obtained previously for local emission-line galaxies but is shifted to higher luminosities and/or lower metallicities compared to that obtained for quiescent irregular dwarf galaxies. For comparison, Lee et al. (2004) have also demonstrated that their 54 H II KISS galaxies with O/H derived with the T_e-method follow the $L - Z$ relation with a slope similar to that for a more quiescent dIrrs but are shifted to higher brightness by 0.8 magnitudes. Furthermore, they have shown that H II galaxies with disturbed irregular outer isophotes (likely due to the interaction) are shifted to a more luminous and/or more metal-poor region in the $L - Z$ diagram as compared to morphologically more regular galaxies. Note that their samples of H II galaxies and of dIrrs are in the same luminosity range as our sample. Papaderos et al. (2008) also note that in contrast to the majority (>90%) of BCDs, the extremely metal-poor SF dwarfs reveal more irregular and bluer hosts.

Thus, the difference in the zero point between our $L - Z$ relation for low-metallicity galaxies and for other galaxies seems to be primarily due to the differences in the intrinsic properties of the galaxies selected for different samples with various selection criteria.

A key question is whether a unique $L - Z$ relation does exist for galaxies of different types. The assessment of this issue is complicated by offsets of high-redshift galaxies with different look-back-times. In this context, Kobulnicky et al. (2003) have shown that both the slopes and zero points of the $L - Z$ relation exhibit a smooth evolution with redshift. A possible universal $L - Z$ relation for galaxies is also blurred by the fact that metallicity determinations of various galaxy samples, differing in their EW(Hβ), absolute magnitude and redshift, do not employ a unique technique. More specifically, several authors emphasize the presence of a well-known shift between the O/H ratio obtained by the direct T_e-method and empirical strong-line methods. Oxygen abundances obtained by empirical methods are by 0.1 –0.25 dex (Shi et al. , 2005) and even by up to 0.6 dex (Hoyos et al. , 2005) higher than those obtained with the T_e-method. For our sample we obtained an offset of ~0.3–0.5 dex.

It can be seen from Fig. 9 that the high-redshift galaxies with an oxygen abundance derived by the T_e-method have a shallower slope compared to local galaxies. On the other hand, oxygen abundances of high-redshift galaxies obtained with the R_{23} empirical strong-line method (data in Fig. 9 by Lilly et al. , 2003;

Kobulnicky & Kewley , 2004; Liang et al. , 2004) are higher and follow the relation for high-metallicity SDSS galaxies in Fig. 7b despite the fact that oxygen abundances for the latter galaxies were calculated with the different semi-empirical strong-line method. Because of this agreement we decided not to recalculate oxygen abundances of high-redshift galaxies with the semi-empirical method and adopted O/H values from the literature. Keeping in mind the systematic differences between oxygen abundances derived with the empirical and the T_e-methods, it might be worth considering a decrease in oxygen abundance by $\sim 0.2 - 0.6$ dex for all high-redshift galaxies with O/H derived with the empirical method. In that case, the position of high-redshift galaxies on the $L - Z$ diagram would be consistent with that of the "branch" galaxies. Such considerations add further support to the results obtained by Pilyugin et al. (2004) and Shi et al. (2005) that the more luminous galaxies have a slope of the $L - Z$ relation more shallow than that of the dwarf galaxies.

We presume that our $L - Z$ relation could be useful as a local reference for studies of this relation for other types of local galaxies and/or of high-redshift galaxies.

5. Summary

We present VLT spectroscopic observations of a new sample of 28 H II regions from 16 emission-line galaxies and ESO 3.6m telescope spectroscopic observations of a new sample of 38 H II regions from 28 emission-line galaxies. These galaxies have mainly been selected from the Data Release 6 (DR6) of the Sloan Digital Sky Survey (SDSS) as low-metallicity galaxy candidates.

Physical conditions and element abundances are derived with the T_e-method for 38 H II regions observed with the 3.6m telescope and for 23 H II regions observed with the VLT.

From our new observations we find that the oxygen abundance in 61 out of the 66 observed H II in our sample ranges from 12 + log O/H = 7.05 to 8.22. The oxygen abundance in 27 H II regions is 12 + log O/H < 7.6 and among them 10 H II regions have an oxygen abundance less than 7.3.

This new data in combination with objects from our previous studies constitute a large uniform sample of 154 H II regions with high-quality spectroscopic data which are used to study the luminosity-metallicity ($L-Z$) relation for the local galaxies with emphasis on its low-metallicity end.

As a comparison sample we use $\sim$ 9000 SDSS emission-line galaxies with higher oxygen abundances which are also obtained mainly by the direct T_e-method. For all of our sample galaxies the g magnitudes are taken from the SDSS while the distances are from the NED. The entire sample spans nearly two orders of magnitude with respect to its gas-phase metallicity, from 12 + log O/H $\sim$ 7.0 to $\sim$ 8.8, and covers an absolute magnitude range from $M_g \sim -12$ to ~ -20.

We find that the metallicity-luminosity relation for our galaxies is consistent with previous ones obtained for objects of similar type. The local $L - Z$ relation obtained with high-quality spectroscopic data is useful for predictions of galaxy evolution models.

Acknowledgements. N. G. G. and Y. I. I. thank the Max Planck Institute for Radioastronomy (MPIfR) for hospitality, and acknowledge support through DFG grant No. Fr 325/57-1. P. P. thanks the Department of Astronomy and Space Physics at Uppsala University for its warm hospitality. K. J. Fricke thanks the MPIfR for Visiting Contracts during 2008 and 2009. This research was partially funded by project grant AYA2007-67965-C03-02 of the Spanish Ministerio de Ciencia e Innovacion. We acknowledge the work of the Sloan Digital Sky Survey (SDSS) team. Funding for the SDSS has been provided by the Alfred P. Sloan Foundation, the Participating Institutions, the National Aeronautics and Space Administration, the National Science Foundation, the US Department of Energy, the Japanese Monbukagakusho, and the Max Planck Society. The SDSS Web site is http:// www.sdss.org/.

References

Abazajian, K., et al. 2009, ApJS, 182, 543

Contini, T., Treyer, M. A., Sullivan, M., & Ellis, R. S. 2002, MNRAS, 330, 75

Ellison, S. L., Patton, D. R., Simard, L., & McConnachie, A. W. 2008, AJ, 135, 1877

Gavilán, M., Mollá, M., & Díaz, Á. 2009, to appear in *Star-forming Dwarf Galaxies: Following Ariadnes Thread in the Cosmic Labyrinth*; preprint: arXiv0902.4695

Gil de Paz, A., Madore, B. F., & Pevunova, O. 2003, ApJS, 147, 29

Guseva, N. G., Izotov, Y. I., Papaderos, P., & Fricke, K. J. 2007, A&A, 464, 885

Hoyos, C., Koo, D. C., Phillips, A. C., Willmer, C. N. A., & Guhathakurta, P. 2005, ApJ, 635, L21

Izotov, Y. I., Lipovetsky, V. A., Chaffee, F. H., Foltz, C. B., Guseva, N. G., & Kniazev, A. Y. 1997, ApJ, 476, 698

Izotov, Y. I., & Thuan, T. X. 2004, ApJ, 602, 200

Izotov, Y. I. & Thuan, T. X. 2007, ApJ, 665, 1115

Izotov, Y. I., Noeske, K. G., Guseva, N. G., Papaderos, P., Thuan, T. X. & Fricke, K. J. 2004a, A&A, 415, L27

Izotov, Y. I., Stasińska, G., Guseva, N. G., & Thuan, T. X. 2004b, A&A, 415, 87

Izotov, Y. I., Stasińska, G., Meynet, G., Guseva, N. G., & Thuan, T. X. 2006a, A&A, 448, 955

Izotov, Y. I., Papaderos, P., Guseva, N. G., Fricke, K. J., & Thuan, T. X. 2006b, A&A, 454, 137

Kakazu, Y., Cowie, L. L., & Hu, E. M. 2007, ApJ, 668, 853

Kewley, L. J., & Dopita, M. A. 2002, ApJS,142, 35

Kewley, L. J., Brown, W. R., Geller, M. J., Kenyon, S. J., & Kurtz, M. J. 2007, AJ, 133, 882

Kobulnicky, H. A., & Zaritsky, D. 1999, ApJ, 511, 118

Kobulnicky, H. A., & Koo, D. C. 2000, ApJ, 545, 712

Kobulnicky, H. A., & Kewley, L. J. 2004, ApJ, 617, 240

Kobulnicky, H. A., Willmer, C. N. A., Phillips, A. C., et al. 2003, ApJ, 599, 1006

Kunth, D., & Östlin, G. 2000, Astron Astrophys Rev, 10, 1

Lamareille, F., Mouhcine, M., Contini, T., Lewis, L., & Maddox, S. 2004, MNRAS, 350, 396

Lee, H, Skillman, E. D., Cannon, J. M., et al. 2006, ApJ, 647, 970

Lee, J. C., Salzer, J. J., & Melbourne, J. 2004, ApJ, 616, 752

Lequeux, J., Rayo, J. F., Serrano, A., Peimbert, M., & Torres-Peimbert, S. 1979, A&A, 80, 155

Liang, Y. C., Hammer, F., Flores, H., Elbaz, D., Marcillac, D., & Cesarsky, C. J. 2004, A&A, 423, 867

Lilly, S. J., Carollo, C. M., & Stockton, A. N. 2003, ApJ, 597, 730

Maier, C., Meisenheimer, K., & Hippelein, H. 2004, A&A, 418, 475

Melbourne, J., & Salzer, J. J. 2002, AJ, 123, 2302

Noeske, K.G., Papaderos, P., Cairos, L.M., & Fricke, K.J. 2003, A&A, 410, 481

Papaderos, P., Loose, H.-H., Fricke, K. J., & Thuan, T. X. 1996, A&A, 314, 59
Papaderos, P., Izotov, Y. I., Fricke, K. J., Thuan, T. X., & Guseva, N. G. 1998, A&A, 338, 43
Papaderos, P., Izotov, Y. I., Thuan, T. X., Noeske, K. G., Fricke, K. J., Guseva, N. G., & Green, R. F. 2002, A&A, 393, 461
Papaderos, P., Guseva, N. G., Izotov, Y. I., & Fricke, K. J. 2008, A&A, 491, 113
Pettini, M., Shapley, A. E., Steidel, C. C., et al. 2001, ApJ, 554, 981
Pilyugin, L. S., Vílchez, J. M., & Contini, T. 2004, A&A, 425, 849
Pilyugin, L. S., Thuan, T. X., & Vílchez, J. M. 2007, MNRAS, 367, 1139
Pilyugin, L. S., Thuan, T. X., & Vílchez, J. M. 2007, MNRAS, 376, 353
Richer, M. G., & MacCall, M. L. 1995, ApJ, 445, 642
Salzer, J. J., MacAlpine, G. M., & Boroson, T. A. 1989, ApJS, 70, 479
Salzer, J. J., Lee, J. C., Melbourne, J., et al. 2005, ApJ, 624, 661
Saviane, I., Ivanov, V. D., Held, E. V., et al. 2008, A&A, 487, 901
Shi, F., Kong, X., Li, C., & Cheng, F. Z. 2005, A&A, 437, 849
Skillman, E. D., Kennicutt, R. C., Jr. & Hodge, P. W. 1989, ApJ, 347, 875
Smith, B. J., & Hancock, M. 2009, AJ, 138, 130
Stasińska, G. 2002, RMxAC, 12, 62
Stasińska, G., & Izotov, Y. I. 2003, A&A, 397, 71
Thuan, T. X., & Izotov, Y. I. 2005, ApJS, 161, 240
Tremonti, C. A., Heckman, T. M., Kauffmann, G., et al. 2004, ApJ, 613, 898
Vanzi, L., Hunt, L.K., Thuan, T.X., & Izotov, Y.I. 2000, A&A, 363, 493
Vaduvescu, O., McCall, M.L., & Richer, M.G. 2007, AJ, 134, 604
Vila-Costas, M. B., & Edmunds, M. G. 1992, MNRAS, 259, 121
Villar-Martín, M., Cerviño, M, & González Delgado, R. M. 2004, MNRAS, 355, 1132
Whitford, A. E. 1958, AJ, 63, 201
Zackrisson, E., Bergvall, N.,& Leitet, E. 2008, ApJ, 676, L9

Table 1. List of galaxies observed with the 3.6m ESO telescope

Galaxy	R.A., Dec. (J2000)	Date (2007)	Exp. time (sec)	Airmass	seeing	redshift
J0015+0104	$00^h15^m20^s.7$, $01°04'37''$	14 Sep	4×900	1.207	1.″74	0.00689 ± 0.00021
J0016+0108	00 16 28. 3, 01 08 02	15 Sep	4×675	1.306	1.″90	0.01035 ± 0.00006
J0029-0108	00 29 04. 7, –01 08 26	16 Sep	4×450	1.614	1.″88	0.01313 ± 0.00006
J0029-0025	00 29 49. 5, –00 25 40	14 Sep	4×900	1.142	1.″72	0.01440 ± 0.00013
0057-0022	00 57 12. 6, –00 21 58	16 Sep	4×900	1.525	1.″47	0.00956 ± 0.00023
J0107+0001	01 07 50. 8, 00 01 28	16 Sep	3×267	1.188	1.″41	0.01835 ± 0.00012
J0109+0107	01 09 08. 0, 01 07 16	15 Sep	4×900	1.174	1.″54	0.00396 ± 0.00013
J0126-0038 No.1	01 26 46. 1, –00 38 39	16 Sep	4×900	1.332	1.″36	0.00632 ± 0.00010
J0126-0038 No.2	01 26 46. 1, –00 38 39	16 Sep	4×900	1.332	1.″36	0.00642 ± 0.00016
J0135-0023	01 35 44. 0, –00 23 17	14 Sep	4×900	1.142	2.″33	0.01708 ± 0.00006
J0213-0002 No.1	02 13 57. 7, –00 02 56	16 Sep	4×900	1.252	1.″52	0.03640 ± 0.00008
J0213-0002 No.2	02 13 57. 7, –00 02 56	16 Sep	4×900	1.252	1.″52	0.03635 ± 0.00011
J0216+0115 No.1	02 16 29. 3, –01 15 21	15 Sep	4×900	1.223	2.″02	0.00939 ± 0.00004
J0216+0115 No.2	02 16 29. 3, 01 15 21	15 Sep	4×900	1.223	2.″02	0.00940 ± 0.00004
096632	02 51 47. 5, –30 06 32	15 Sep	4×900	1.400	2.″28	0.00354 ± 0.00009
J0252+0017	02 52 16. 8, 00 17 41	16 Sep	3×800	1.165	1.″38	0.00527 ± 0.00011
J0256+0036	02 56 28. 3, 00 36 28	14 Sep	4×900	1.150	2.″47	0.00919 ± 0.00013
J0303-0109 No.1	03 03 31. 3, –01 09 47	14 Sep	2×800	1.170	2.″43	0.03055 ± 0.00011
J0303-0109 No.2	03 03 31. 3, –01 09 47	14 Sep	2×800	1.170	2.″43	0.03039 ± 0.00017
J0341-0026 No.1	03 41 18. 1, -00 26 28	16 Sep	3×800	1.198	1.″46	0.03080 ± 0.00020
J0341-0026 No.2	03 41 18. 1, –00 26 28	16 Sep	3×800	1.198	1.″46	0.03045 ± 0.00008
J0341-0026 No.3	03 41 18. 1, –00 26 28	16 Sep	3×800	1.198	1.″46	0.03047 ± 0.00008
G1815456-670126	18 15 46. 5, –67 01 23	14 Sep	4×900	1.280	2.″00	0.01131 ± 0.00008
G2052078-691229 No.1	20 52 07. 1, –69 12 30	16 Sep	3×800	1.328	1.″50	0.00212 ± 0.00008
G2052078-691229 No.2	20 52 07. 1, –69 12 30	16 Sep	3×800	1.328	1.″50	0.00203 ± 0.00011
J2053+0039	20 53 12. 6, 00 39 15	15 Sep	4×525	1.219	1.″55	0.01328 ± 0.00007
J2105+0032 No.1	21 05 08. 6, 00 32 23	14 Sep	3×800	1.408	1.″45	0.01431 ± 0.00003
J2105+0032 No.2	21 05 08. 6, 00 32 23	14 Sep	3×800	1.408	1.″45	0.01436 ± 0.00013
J2112-0016 No.1	21 12 00. 8, –00 16 49	15 Sep	3×800	1.441	1.″32	0.01195 ± 0.00015
J2112-0016 No.2	21 12 00. 8, –00 16 49	15 Sep	3×800	1.441	1.″32	0.01215 ± 0.00021
J2119-0732	21 19 42. 4, –07 32 24	14 Sep	3×800	1.130	1.″78	0.00966 ± 0.00006
J2120-0058	21 20 25. 9, –00 58 27	15 Sep	4×900	1.172	1.″54	0.01979 ± 0.00004
J2150+0033	21 50 32. 0, 00 33 05	15 Sep	3×800	1.155	2.″32	0.01508 ± 0.00003
G2155572-394614	21 55 57. 9, –39 46 14	15 Sep	3×900	1.241	1.″90	0.00740 ± 0.00008
J2227-0939	22 27 30. 7, –09 39 54	14 Sep	3×800	1.060	2.″14	0.00528 ± 0.00007
PHL 293B	22 30 36. 8, –00 06 37	14 Sep	4×900	1.230	1.″35	0.00537 ± 0.00004
J2310-0109 No.1	23 10 42. 0, –01 09 48	16 Sep	3×800	1.471	1.″45	0.01254 ± 0.00008
J2310-0109 No.2	23 10 42. 0, –01 09 48	16 Sep	3×800	1.471	1.″45	0.01232 ± 0.00009

Table 2. List of galaxies observed with the VLT[a]

Galaxy	R.A., Dec. (J2000)	Date	Exp. time (sec)	Airmass	seeing	redshift
J0004+0025 No.1	$00^h04^m21^s.6$, $00°25'36''$	20.10.2006	2 × 750	1.246	0″.60	0.01269 ± 0.00004
			2 × 540	1.181	0″.37	0.01269 ± 0.00004
J0004+0025 No.2	00 04 21. 6, 00 25 36	20.10.2006	2 × 750	1.246	0″.60	0.01266 ± 0.00003
			2 × 540	1.181	0″.37	0.01266 ± 0.00003
J0014-0044 No.1	00 14 28. 8, –00 44 44	19.11.2006	2 × 750	1.158	1″.22	0.01361 ± 0.00004
			2 × 540	1.217	0″.93	0.01361 ± 0.00004
J0014-0044 No.2	00 14 28. 8, –00 44 44	19.11.2006	2 × 750	1.158	1″.22	0.01379 ± 0.00002
			2 × 540	1.217	0″.93	0.01379 ± 0.00002
J0202-0047	02 02 38. 0, –00 47 44	13.01.2007	2 × 750	1.211	1″.85	0.03371 ± 0.00003
			2 × 540	1.294	1″.63	0.03371 ± 0.00003
J0301-0059 No.1	03 01 26. 3, –00 59 26	13.12.2006	2 × 750	1.140	1″.46	0.03841 ± 0.00000
			2 × 540	1.191	1″.38	0.03841 ± 0.00000
J0301-0059 No.2	03 01 26. 3, –00 59 26	13.12.2006	2 × 750	1.140	1″.46	0.03822 ± 0.00002
			2 × 540	1.191	1″.38	0.03822 ± 0.00002
J0301-0059 No.3	03 01 26. 3, –00 59 26	13.12.2006	2 × 750	1.140	1″.46	0.03807 ± 0.00008
			2 × 540	1.191	1″.38	0.03807 ± 0.00008
J0315-0024 No.1	03 15 59. 9, –00 24 26	26.11.2006	2 × 1500	1.145	1″.32	0.02247 ± 0.00005
			2 × 1080	1.197	1″.08	0.02247 ± 0.00005
J0315-0024 No.2	03 15 59. 9, –00 24 26	26.11.2006	2 × 1500	1.145	1″.32	0.02261 ± 0.00006
			2 × 1080	1.197	1″.08	0.02261 ± 0.00006
J0338+0013 (BG)	03 38 12. 2, 00 13 13	25.11.2006	2 × 750	1.207	0″.76	0.39695 ± 0.00000
			2 × 540	1.284	0″.70	0.39695 ± 0.00000
J0338+0013	03 38 12. 2, 00 13 13	25.11.2006	2 × 750	1.207	0″.76	0.04266 ± 0.00002
			2 × 540	1.284	0″.70	0.04266 ± 0.00002
G0405204-364859 No.1	04 05 18. 6, –36 48 49	15.11.2006	2 × 750	1.033	1″.11	0.00281 ± 0.00004
			2 × 540	1.054	1″.00	0.00281 ± 0.00004
G0405204-364859 No.2	04 05 18. 6, –36 48 49	15.11.2006	2 × 750	1.033	1″.11	0.00275 ± 0.00003
			2 × 540	1.054	1″.00	0.00275 ± 0.00003
G0405204-364859 No.3	04 05 18. 6, –36 48 49	15.11.2006	2 × 750	1.033	1″.11	0.00276 ± 0.00003
			2 × 540	1.054	1″.00	0.00276 ± 0.00003
G0405204-364859 (BG)	04 05 18. 6, –36 48 49	15.11.2006	2 × 750	1.033	1″.11	0.17236 ± 0.00000
			2 × 540	1.054	1″.00	0.17236 ± 0.00000
J0519+0007	05 19 02. 7, 00 07 29	16.11.2006	2 × 750	1.220	1″.03	0.04438 ± 0.00002
			2 × 540	1.166	1″.27	0.04438 ± 0.00002
J2104-0035 No.1	21 04 55. 3, –00 35 22	12.10.2006	2 × 750	1.099	1″.48	0.00469 ± 0.00002
			2 × 540	1.096	1″.40	0.00469 ± 0.00002
J2104-0035 No.2	21 04 55. 3, –00 35 22	12.10.2006	2 × 750	1.099	1″.48	0.00469 ± 0.00001
			2 × 540	1.096	1″.40	0.00469 ± 0.00001
J2104-0035 No.3	21 04 55. 3, –00 35 22	12.10.2006	2 × 750	1.099	1″.48	0.00471 ± 0.00005
			2 × 540	1.096	1″.40	0.00471 ± 0.00005
J2104-0035 No.4	21 04 55. 3, –00 35 22	12.10.2006	2 × 750	1.099	1″.48	0.00472 ± 0.00003
			2 × 540	1.096	1″.40	0.00472 ± 0.00003
J2302+0049 No.1	23 02 10. 0, 00 49 39	12.10.2006	2 × 750	1.170	1″.18	0.03312 ± 0.00002
			2 × 540	1.132	1″.23	0.03312 ± 0.00002
J2302+0049 No.2	23 02 10. 0, 00 49 39	12.10.2006	2 × 750	1.170	1″.18	0.03311 ± 0.00002
			2 × 540	1.132	1″.23	0.03311 ± 0.00002
J2324-0006	23 24 21. 3, –00 06 29	12.10.2006	2 × 750	1.102	1″.55	0.00896 ± 0.00002
			2 × 540	1.119	1″.53	0.00896 ± 0.00002
J2354-0005 No.1	23 54 37. 3, –00 05 02	15.10.2006	2 × 1500	1.502	0″.74	0.00771 ± 0.00003
			2 × 1080	1.362	0″.77	0.00771 ± 0.00003
J2354-0005 No.2	23 54 37. 3, –00 05 02	15.10.2006	2 × 1500	1.502	0″.74	0.00798 ± 0.00004
			2 × 1080	1.362	0″.77	0.00798 ± 0.00004
J2354-0005 (BG1)	23 54 37. 3, –00 05 02	15.10.2006	2 × 1500	1.502	0″.74	0.16534 ± 0.00000
			2 × 1080	1.362	0″.77	0.16534 ± 0.00000
J2354-0005 (BG2)	23 54 37. 3, –00 05 02	15.10.2006	2 × 1500	1.502	0″.74	0.16520 ± 0.00000
			2 × 1080	1.362	0″.77	0.16520 ± 0.00000

[a] first line for each galaxy is related to the observation in the blue range and second line to the one in the red range.

Table 3. Emission line intensities (3.6m ESO observations)

Ion	$I(\lambda)/I(H\beta)$	$I(\lambda)/I(H\beta)$	$I(\lambda)/I(H\beta)$	$I(\lambda)/I(H\beta)$	$I(\lambda)/I(H\beta)$	$I(\lambda)/I(H\beta)$	$I(\lambda)/I(H\beta)$	$I(\lambda)/I(H\beta)$
	GALAXY							
	J0015+0104	J0016+0108	J0029−0108	J0029−0025	J0057−0022	J0107+0001	J0109+0107	J0126−0038 No.1
3727 [O II]	118.7 ± 5.7	221.2 ± 7.8	171.6 ± 30.8	130.3 ± 7.8	219.7 ± 5.4	162.3 ± 13.6	209.3 ± 4.3	238.1 ± 4.1
3868 [Ne III]	...	...	...	...	31.0 ± 2.0	...	30.1 ± 1.0	38.5 ± 0.9
3889 He I + H8	...	...	...	...	17.3 ± 1.8	...	20.6 ± 1.6	17.2 ± 0.9
3968 [Ne III] + H7	...	...	...	...	16.1 ± 1.9	...	25.6 ± 1.5	22.2 ± 0.9
4101 Hδ	...	...	...	...	24.9 ± 1.9	...	24.9 ± 1.3	24.8 ± 0.9
4340 Hγ	49.3 ± 3.5	47.0 ± 3.4	...	43.9 ± 4.8	47.2 ± 1.9	...	46.9 ± 1.4	46.9 ± 1.0
4363 [O III]	...	...	...	...	5.1 ± 0.1	...	3.7 ± 0.4	6.9 ± 0.4
4471 He I	...	...	...	...	...	...	2.6 ± 0.4	2.4 ± 0.3
4658 [Fe III]	...	...	...	...	...	...	...	1.5 ± 0.3
4686 He II	...	...	...	...	...	...	...	1.7 ± 0.3
4861 Hβ	100.0 ± 4.9	100.0 ± 4.2	100.0 ± 15.0	100.0 ± 6.2	100.0 ± 2.6	100.0 ± 8.0	100.0 ± 2.1	100.0 ± 1.7
4959 [O III]	20.1 ± 2.0	61.1 ± 2.8	48.1 ± 8.8	38.8 ± 3.2	76.1 ± 2.0	31.0 ± 3.3	102.5 ± 2.1	139.7 ± 2.3
5007 [O III]	57.8 ± 2.8	190.6 ± 6.1	144.3 ± 22.7	168.6 ± 7.9	219.4 ± 4.8	93.1 ± 7.9	305.1 ± 5.6	409.4 ± 6.4
$C(H\beta)^a$	0.000	0.000	0.000	0.000	0.245	0.000	0.120	0.410
$F(H\beta)^b$	2.77	4.66	1.19	2.16	12.99	2.88	18.18	75.47
EW(Hβ) (Å)	57.5	20.4	6.8	53.8	44.6	87.7	50.1	48.7
EW(abs) (Å)^a	0.00	0.00	0.00	2.00	0.25	2.00	2.15	0.70
	GALAXY							
	J0126−0038 No.2	J0135−0023	J0213−0002 No.1	J0213−0002 No.2	J0216+0115 No.1	J0216+0115 No.2	096632	J0252+0017
3727 [O II]	224.9 ± 6.3	177.9 ± 10.0	182.2 ± 9.8	291.0 ± 16.6	225.2 ± 8.7	236.5 ± 12.4	306.5 ± 6.9	257.0 ± 26.1
3868 [Ne III]	...	...	...	...	...	...	8.4 ± 0.9	...
4101 Hδ	24.8 ± 2.2	...	...	...	...	...	29.7 ± 1.7	...
4340 Hγ	44.8 ± 2.2	44.0 ± 5.8	47.1 ± 5.0	47.3 ± 7.3	49.3 ± 3.9	...	48.1 ± 1.8	...
4861 Hβ	100.0 ± 3.0	100.0 ± 6.7	100.0 ± 6.6	100.0 ± 7.6	100.0 ± 4.6	100.0 ± 10.0	100.0 ± 2.4	100.0 ± 10.0
4959 [O III]	59.3 ± 1.9	43.5 ± 3.5	97.0 ± 5.8	115.6 ± 7.2	83.8 ± 3.8	42.1 ± 3.9	35.2 ± 1.2	71.7 ± 8.5
5007 [O III]	170.7 ± 4.3	155.9 ± 7.9	279.2 ± 13.1	332.9 ± 16.7	245.6 ± 8.3	126.9 ± 6.7	100.3 ± 2.3	270.5 ± 24.1
$C(H\beta)^a$	0.000	0.000	0.000	0.000	0.000	0.000	0.000	0.000
$F(H\beta)^b$	7.47	2.87	2.54	1.73	3.11	2.26	10.20	1.69
EW(Hβ) (Å)	45.6	14.0	52.1	36.7	17.2	24.3	48.3	11.1
EW(abs) (Å)^a	2.00	2.00	2.00	0.00	0.00	0.00	2.00	2.00
	GALAXY							
	J0256+0036	J0303−0109 No.1	J0303−0109 No.2	J0341−0026 No.1	J0341−0026 No.2	J0341−0026 No.3	G1815-6701	G2052-6912 No.1
3727 [O II]	190.3 ± 5.1	137.9 ± 4.5	170.4 ± 22.5	227.5 ± 13.6	136.4 ± 5.9	87.5 ± 5.0	263.8 ± 4.4	137.6 ± 2.1
3750 H12	...	...	...	...	...	...	...	3.3 ± 0.2
3771 H11	...	...	...	...	...	...	...	3.8 ± 0.2
3798 H10	...	...	...	...	...	...	...	5.1 ± 0.2
3835 H9	...	...	...	...	...	...	...	7.1 ± 0.2
3868 [Ne III]	31.7 ± 1.7	42.9 ± 2.2	...	...	...	...	52.3 ± 1.1	37.2 ± 0.6
3889 He I + H8	...	30.6 ± 2.8	...	...	...	...	17.5 ± 0.8	19.3 ± 0.4
3968 [Ne III] + H7	...	36.4 ± 3.0	...	...	...	...	25.7 ± 0.8	27.2 ± 0.5
4026 He I	...	...	...	...	...	...	...	1.5 ± 0.1
4068 [S II]	...	...	...	...	...	...	...	1.3 ± 0.1
4101 Hδ	...	33.8 ± 2.7	...	...	...	...	23.7 ± 0.8	25.9 ± 0.4
4340 Hγ	47.8 ± 2.2	47.0 ± 2.5	...	...	45.4 ± 4.4	50.0 ± 4.7	46.9 ± 1.0	46.6 ± 0.7
4363 [O III]	...	8.2 ± 1.0	...	...	...	...	8.7 ± 0.4	4.1 ± 0.1
4471 He I	...	...	...	...	...	...	3.5 ± 0.4	3.9 ± 0.1
4658 [Fe III]	...	...	...	...	...	...	1.7 ± 0.3	0.3 ± 0.1
4686 He II	...	...	...	...	...	...	1.6 ± 0.4	0.3 ± 0.1
4711 [Ar IV] + He I	...	...	...	...	...	...	...	0.7 ± 0.1
4861 Hβ	100.0 ± 3.0	100.0 ± 3.0	100.0 ± 13.0	100.0 ± 8.0	100.0 ± 4.7	100.0 ± 5.2	100.0 ± 1.7	100.0 ± 1.5
4921 He I	...	...	...	18.9 ± 2.8	...	...	...	0.9 ± 0.1
4959 [O III]	110.1 ± 3.0	130.6 ± 3.5	26.6 ± 5.1	68.0 ± 4.9	77.0 ± 3.5	65.3 ± 3.3	171.5 ± 2.7	160.5 ± 2.3
5007 [O III]	316.2 ± 7.3	368.4 ± 8.9	79.9 ± 11.6	253.6 ± 13.9	243.1 ± 8.4	186.1 ± 7.6	508.6 ± 7.9	481.2 ± 7.0
$C(H\beta)^a$	0.000	0.515	0.000	0.000	0.000	0.000	0.575	0.390
$F(H\beta)^b$	9.25	11.86	1.71	4.49	4.49	3.54	66.43	448.40
EW(Hβ) (Å)	26.2	95.0	21.2	27.5	85.2	145.8	35.9	221.4
EW(abs) (Å)^a	0.00	1.50	2.00	0.00	2.00	2.00	0.40	0.75
	GALAXY							
	G2052-6912 No.2	J2053+0039	J2105+0032 No.1	J2105+0032 No.2	J2112-0016 No.1	J2112-0016 No.2	J2119-0732	J2120-0058
3727 [O II]	104.5 ± 1.6	85.8 ± 8.2	109.0 ± 8.3	187.0 ± 10.8	106.6 ± 2.1	107.6 ± 4.6	161.7 ± 4.1	252.5 ± 5.3
3750 H12	3.5 ± 0.1	...	...	...	...	...	...	...
3771 H11	4.1 ± 0.1	...	...	...	...	...	...	...
3798 H10	5.2 ± 0.2	...	...	...	...	...	...	...
3820 He I	1.1 ± 0.1	...	...	...	...	...	...	...
3835 H9	7.2 ± 0.2	...	...	...	...	...	...	...
3868 [Ne III]	47.9 ± 0.7	...	...	...	42.7 ± 1.0	25.7 ± 2.0	38.5 ± 1.7	39.9 ± 1.4
3889 He I + H8	18.1 ± 0.3	...	...	...	18.4 ± 0.8	18.0 ± 3.1	24.5 ± 2.0	22.5 ± 1.7
3968 [Ne III] + H7	30.9 ± 0.5	...	...	...	27.9 ± 1.0	37.0 ± 3.3	...	20.4 ± 1.7
4026 He I	1.7 ± 0.1	...	...	...	...	...	...	...
4068 [S II]	1.0 ± 0.1	...	...	...	...	...	...	...
4101 Hδ	25.9 ± 0.4	...	...	...	25.8 ± 1.0	41.1 ± 2.4	26.8 ± 1.8	27.5 ± 1.5
4340 Hγ	46.7 ± 0.7	...	...	...	48.7 ± 1.1	46.9 ± 3.0	46.7 ± 1.8	47.2 ± 1.6
4363 [O III]	6.7 ± 0.1	...	...	...	5.3 ± 0.4	5.5 ± 0.9	...	7.8 ± 0.8
4387 He I	0.6 ± 0.1	...	...	...	...	...	...	...

Table 3. continued.

Ion	$I(\lambda)/I(H\beta)$	$I(\lambda)/I(H\beta)$	$I(\lambda)/I(H\beta)$	$I(\lambda)/I(H\beta)$	$I(\lambda)/I(H\beta)$	$I(\lambda)/I(H\beta)$	$I(\lambda)/I(H\beta)$	$I(\lambda)/I(H\beta)$
4471 He I	4.1 ± 0.1	...	...	...	3.7 ± 0.3	...	...	...
4658 [Fe III]	0.2 ± 0.1	...	...	...	...	...	...	...
4711 [Ar IV] + He I	1.4 ± 0.1	...	...	...	...	...	...	...
4740 [Ar IV]	0.6 ± 0.1	...	...	...	...	...	...	...
4861 Hβ	100.0 ± 1.5	100.0 ± 9.0	100.0 ± 8.0	100.0 ± 6.0	100.0 ± 1.8	100.0 ± 3.5	100.0 ± 2.6	100.0 ± 2.2
4921 He I	1.1 ± 0.1	...	...	...	...	...	...	...
4959 [O III]	207.9 ± 3.0	75.2 ± 7.1	71.2 ± 5.3	53.4 ± 4.0	189.9 ± 3.2	152.6 ± 4.7	137.3 ± 3.1	102.4 ± 2.1
5007 [O III]	623.9 ± 9.0	216.5 ± 14.3	263.8 ± 14.4	165.6 ± 8.1	565.0 ± 9.1	454.1 ± 12.5	413.1 ± 8.6	297.6 ± 5.6
$C(H\beta)$[a]	0.495	0.000	0.000	0.000	0.000	0.245	0.095	0.415
$F(H\beta)$[b]	766.20	1.58	2.57	2.36	49.75	7.37	16.82	15.15
EW(Hβ) (Å)	395.9	24.4	18.2	121.7	95.2	176.1	52.8	40.1
EW(abs) (Å)[a]	1.00	2.00	2.00	2.00	0.00	4.15	2.00	0.90

	Galaxy					
	J2150+0033	G2155-3946	J2227-0939	PHL 293B	J2310-0109 No.1	J2310-0109 No.2
3727 [O II]	190.0 ± 7.3	323.4 ± 10.2	197.0 ± 7.0	65.7 ± 1.1	128.0 ± 4.0	177.4 ± 6.0
3750 H12	...	...	...	5.0 ± 0.4	...	...
3771 H11	...	...	...	6.4 ± 0.4	...	...
3798 H10	...	...	...	8.2 ± 0.4	...	...
3835 H9	...	...	...	8.4 ± 0.4	...	...
3868 [Ne III]	...	16.6 ± 1.9	35.0 ± 3.0	41.0 ± 0.7	20.9 ± 1.4	27.8 ± 1.9
3889 He I + H8	...	...	23.4 ± 7.2	21.4 ± 0.5	...	...
3968 [Ne III] + H7	...	...	26.9 ± 4.9	28.9 ± 0.6	...	...
4101 Hδ	...	22.8 ± 4.6	28.5 ± 4.4	25.7 ± 0.5	...	...
4340 Hγ	39.9 ± 3.4	47.1 ± 3.0	47.3 ± 3.4	47.4 ± 0.8	38.3 ± 2.7	41.5 ± 3.4
4363 [O III]	7.3 ± 1.3	...	...	12.3 ± 0.3	...	8.7 ± 1.3
4471 He I	...	...	...	3.5 ± 0.2	...	...
4686 He II	...	...	...	1.4 ± 0.1	...	...
4711 [Ar IV] + He I	...	...	...	1.8 ± 0.1	...	...
4740 [Ar IV]	...	...	...	1.1 ± 0.1	...	...
4861 Hβ	100.0 ± 4.6	100.0 ± 3.8	100.0 ± 3.9	100.0 ± 1.5	100.0 ± 3.3	100.0 ± 3.8
4959 [O III]	86.9 ± 3.5	59.3 ± 2.4	128.2 ± 4.3	157.1 ± 2.4	122.1 ± 3.4	115.5 ± 3.7
5007 [O III]	255.9 ± 8.4	170.9 ± 5.1	373.0 ± 10.9	466.7 ± 7.0	369.4 ± 9.0	332.8 ± 9.2
$C(H\beta)$[a]	0.000	0.000	0.000	0.305	0.000	0.000
$F(H\beta)$[b]	4.59	10.53	21.39	107.50	14.00	9.26
EW(Hβ) (Å)	30.0	13.8	20.3	117.2	26.1	30.5
EW(abs) (Å)[a]	2.00	2.00	2.00	1.50	2.00	2.00

[a] zero value is assumed if a negative value is derived.

[b] in units of 10^{-16} erg s^{-1} cm^{-2}.

Table 4. Emission line intensities (VLT observations)

Ion	$I(\lambda)/I(\mathrm{H}\beta)$	$I(\lambda)/I(\mathrm{H}\beta)$	$I(\lambda)/I(\mathrm{H}\beta)$	$I(\lambda)/I(\mathrm{H}\beta)$	$I(\lambda)/I(\mathrm{H}\beta)$	$I(\lambda)/I(\mathrm{H}\beta)$	$I(\lambda)/I(\mathrm{H}\beta)$	$I(\lambda)/I(\mathrm{H}\beta)$
	GALAXY							
	J0004+0025	J0004+0025	J0014−0044	J0014−0044	J0202−0047	J0301−0059	J0301−0059	J0301−0059
	No.1	No.2	No.1	No.2		No.1	No.2	No.3
3727 [O II]	214.05 ± 11.27	253.26 ± 13.99	99.16 ± 1.73	298.77 ± 9.30	191.81 ± 3.50	331.24 ± 6.29	304.43 ± 6.86	330.51 ± 21.26
3750 H12	...	...	4.57 ± 0.56	...	...	...	...	...
3771 H11	...	...	5.06 ± 0.52	...	4.22 ± 0.66	...	...	...
3798 H10	...	...	7.06 ± 0.52	...	4.83 ± 0.67	...	...	...
3835 H9	...	...	8.66 ± 0.46	...	5.85 ± 0.58	...	...	...
3868 [Ne III]	...	33.25 ± 4.96	50.11 ± 0.85	...	41.34 ± 0.92	24.06 ± 0.98	23.23 ± 1.72	...
3889 He I + H8	...	...	21.72 ± 0.55	...	22.44 ± 0.72	22.59 ± 1.80	...	...
3968 [Ne III] + H7	...	...	32.07 ± 0.64	...	28.21 ± 0.78	25.37 ± 1.37	...	...
4026 He I	...	...	1.10 ± 0.11	...	...	...	...	...
4101 Hδ	...	...	25.84 ± 0.51	28.41 ± 2.21	25.71 ± 0.70	28.75 ± 1.16	28.14 ± 2.37	...
4340 Hγ	47.25 ± 3.35	47.74 ± 3.21	46.79 ± 0.77	51.88 ± 1.98	48.61 ± 0.93	46.88 ± 1.15	45.15 ± 1.68	...
4363 [O III]	...	...	8.87 ± 0.18	...	8.97 ± 0.37	3.46 ± 0.42	4.43 ± 0.92	...
4387 He I	...	...	0.57 ± 0.08	...	...	...	...	...
4471 He I	...	...	3.83 ± 0.12	...	3.49 ± 0.26	...	...	...
4711 [Ar IV] + He I	...	...	1.08 ± 0.09	...	...	...	...	...
4740 [Ar IV]	...	...	0.84 ± 0.07	...	...	...	...	...
4861 Hβ	100.00 ± 3.77	100.00 ± 3.98	100.00 ± 1.49	100.00 ± 2.52	100.00 ± 1.60	100.00 ± 1.81	100.00 ± 2.17	100.00 ± 17.01
4921 He I	...	...	0.94 ± 0.06	...	...	...	...	...
4959 [O III]	37.84 ± 1.98	62.06 ± 2.64	207.93 ± 3.04	59.47 ± 1.64	161.71 ± 2.50	91.37 ± 1.62	90.51 ± 1.93	53.80 ± 4.75
4988 [Fe III]	...	...	0.44 ± 0.01	...	...	...	...	...
5007 [O III]	108.99 ± 3.45	183.91 ± 5.64	621.54 ± 9.04	175.13 ± 3.94	495.48 ± 7.53	275.10 ± 4.60	267.82 ± 5.17	154.51 ± 8.64
5015 He I	...	...	0.90 ± 0.03	...	2.20 ± 0.15	...	...	...
5518 [Cl III]	...	...	0.38 ± 0.06	...	...	...	...	...
5538 [Cl III]	...	...	0.61 ± 0.10	...	...	...	...	...
5876 He I	...	...	10.92 ± 0.19	13.81 ± 0.29	10.96 ± 0.27	9.94 ± 0.61	11.70 ± 0.82	...
6300 [O I]	...	...	1.92 ± 0.06	...	3.11 ± 0.13	9.14 ± 0.52	9.57 ± 0.60	...
6312 [S III]	...	...	1.73 ± 0.06	...	1.74 ± 0.11	0.97 ± 0.02	...	...
6363 [O I]	...	...	0.70 ± 0.05	...	1.42 ± 0.02	2.73 ± 0.40	2.72 ± 0.05	...
6548 [N II]	...	...	2.16 ± 0.06	10.39 ± 0.88	3.86 ± 0.13	6.66 ± 0.44	7.77 ± 0.53	...
6563 Hα	269.07 ± 8.14	266.58 ± 8.43	283.02 ± 4.47	288.13 ± 6.59	281.45 ± 4.63	284.02 ± 5.14	281.73 ± 5.83	288.79 ± 19.92
6583 [N II]	15.55 ± 1.51	12.75 ± 1.07	5.73 ± 0.11	22.66 ± 0.99	9.59 ± 0.21	20.47 ± 0.54	26.57 ± 0.81	33.85 ± 3.43
6678 He I	...	...	3.05 ± 0.07	...	2.69 ± 0.11	1.83 ± 0.35	...	...
6717 [S II]	32.18 ± 1.51	27.90 ± 1.41	8.04 ± 0.14	31.47 ± 1.01	16.63 ± 0.32	42.25 ± 0.88	47.03 ± 1.11	63.87 ± 4.85
6731 [S II]	25.79 ± 1.51	22.66 ± 1.32	5.78 ± 0.11	24.87 ± 0.91	12.38 ± 0.26	29.45 ± 0.68	32.66 ± 0.86	44.23 ± 4.15
7065 He I	...	...	2.45 ± 0.06	...	1.66 ± 0.09	1.58 ± 0.26	...	...
7136 [Ar III]	...	...	6.61 ± 0.12	...	8.26 ± 0.19	6.60 ± 0.41	7.65 ± 0.41	...
7281 He I	...	...	0.51 ± 0.03	...	0.92 ± 0.08	...	...	...
7320 [O II]	...	...	1.51 ± 0.05	...	2.16 ± 0.09	...	...	...
7330 [O II]	...	...	1.36 ± 0.05	...	1.85 ± 0.07	...	...	...
$C(\mathrm{H}\beta)^a$	0.000	0.000	0.210	0.030	0.305	0.215	0.185	0.110
$F(\mathrm{H}\beta)^b$	0.76	0.80	20.90	0.81	5.47	5.40	3.59	0.38
EW(Hβ) (Å)	22.5	21.4	275.7	74.2	132.6	28.3	13.6	8.0
EW(abs) (Å)	2.00	2.00	2.20	2.00	0.50	1.95	1.75	2.00
	GALAXY							
	J0315−0024	J0315−0024	J0338+0013	G0405-3648	G0405-3648	G0405-3648	J0519+0007	J2104−0035
	No.1	No.2		No.1	No.2	No.3		No.1
3727 [O II]	174.28 ± 5.19	190.40 ± 9.12	60.18 ± 1.06	129.50 ± 5.31	160.45 ± 3.75	154.37 ± 3.90	27.98 ± 0.47	27.37 ± 0.97
3750 H12	...	...	3.59 ± 0.30	...	...	...	3.13 ± 0.18	4.11 ± 0.75
3771 H11	...	...	3.80 ± 0.29	...	...	...	4.07 ± 0.18	5.22 ± 0.73
3798 H10	...	...	6.86 ± 0.30	...	...	...	5.75 ± 0.18	6.80 ± 0.66
3820 He I	...	...	2.00 ± 0.18	...	...	...	0.74 ± 0.09	...
3835 H9	...	...	8.51 ± 0.28	...	...	...	7.26 ± 0.19	8.01 ± 0.61
3868 [Ne III]	8.88 ± 1.88	...	41.54 ± 0.71	9.66 ± 1.46	11.59 ± 1.16	14.90 ± 1.09	35.86 ± 0.56	24.32 ± 0.53
3889 He I + H8	20.76 ± 2.11	...	18.64 ± 0.41	18.38 ± 3.37	18.70 ± 1.09	20.05 ± 1.24	17.21 ± 0.31	22.61 ± 0.66
3968 [Ne III] + H7	16.88 ± 1.83	...	28.87 ± 0.53	17.38 ± 2.88	15.71 ± 1.02	20.71 ± 1.21	26.96 ± 0.44	23.31 ± 0.65
4026 He I	...	...	2.82 ± 0.17	...	...	...	1.55 ± 0.08	2.12 ± 0.18
4068 [S II]	...	...	1.16 ± 0.02	...	...	...	0.65 ± 0.06	...
4101 Hδ	21.87 ± 1.58	...	26.20 ± 0.47	25.79 ± 1.85	21.62 ± 0.82	24.52 ± 0.99	25.67 ± 0.41	25.83 ± 0.63
4227 [Fe V]	...	...	...	...	...	...	0.86 ± 0.14	...
4340 Hγ	49.15 ± 1.56	50.73 ± 4.71	48.06 ± 0.76	47.97 ± 1.55	45.48 ± 1.00	49.12 ± 1.13	47.62 ± 0.71	48.28 ± 0.82
4363 [O III]	2.04 ± 0.74	...	14.66 ± 0.27	4.02 ± 0.76	4.03 ± 0.36	5.12 ± 0.50	15.04 ± 0.24	9.87 ± 0.20
4387 He I	...	...	...	...	...	...	0.37 ± 0.05	...
4471 He I	...	...	3.70 ± 0.13	2.18 ± 0.72	3.54 ± 0.43	2.63 ± 0.40	3.60 ± 0.08	3.65 ± 0.13
4658 [Fe III]	...	...	0.49 ± 0.06	...	...	...	0.49 ± 0.04	...
4686 He II	...	...	1.15 ± 0.08	...	...	...	1.52 ± 0.05	0.65 ± 0.10
4711 [Ar IV] + He I	...	...	2.35 ± 0.09	...	...	...	2.33 ± 0.06	1.52 ± 0.09
4740 [Ar IV]	...	...	1.40 ± 0.07	...	...	...	1.51 ± 0.06	0.74 ± 0.10
4861 Hβ	100.00 ± 1.95	100.00 ± 4.69	100.00 ± 1.48	100.00 ± 2.03	100.00 ± 1.70	100.00 ± 1.77	100.00 ± 1.44	100.00 ± 1.50
4921 He I	...	...	1.27 ± 0.08	...	...	...	0.98 ± 0.05	1.11 ± 0.08
4959 [O III]	53.68 ± 1.19	51.95 ± 2.12	176.71 ± 2.58	70.62 ± 1.51	48.62 ± 0.91	45.69 ± 0.93	148.33 ± 2.13	96.10 ± 1.41
4988 [Fe III]	...	...	0.54 ± 0.05	...	1.96 ± 0.31	...	0.65 ± 0.04	0.75 ± 0.13
5007 [O III]	162.82 ± 2.95	151.44 ± 4.43	530.20 ± 7.71	206.51 ± 3.80	140.34 ± 2.29	137.62 ± 2.33	439.62 ± 6.30	288.91 ± 4.20
5015 He I	...	...	2.59 ± 0.08	...	...	...	0.97 ± 0.04	1.64 ± 0.18
5755 [N II]	...	...	...	...	...	...	0.15 ± 0.02	...
5876 He I	9.03 ± 0.55	...	11.14 ± 0.21	8.41 ± 0.58	9.77 ± 0.48	5.72 ± 0.29	11.60 ± 0.18	9.38 ± 0.19
6300 [O I]	...	...	1.72 ± 0.07	...	4.36 ± 0.36	2.75 ± 0.25	1.07 ± 0.03	0.49 ± 0.06
6312 [S III]	...	...	1.01 ± 0.07	...	...	...	0.78 ± 0.02	0.66 ± 0.06
6363 [O I]	...	...	0.53 ± 0.05	...	...	...	0.37 ± 0.02	...
6548 [N II]	...	...	...	...	...	...	1.17 ± 0.03	...
6563 Hα	283.73 ± 5.33	288.03 ± 8.76	277.02 ± 4.37	279.40 ± 5.45	275.30 ± 4.73	272.50 ± 4.83	274.85 ± 4.27	274.51 ± 4.32

Table 4. continued.

Ion	$I(\lambda)/I(\mathrm{H}\beta)$	$I(\lambda)/I(\mathrm{H}\beta)$	$I(\lambda)/I(\mathrm{H}\beta)$	$I(\lambda)/I(\mathrm{H}\beta)$	$I(\lambda)/I(\mathrm{H}\beta)$	$I(\lambda)/I(\mathrm{H}\beta)$	$I(\lambda)/I(\mathrm{H}\beta)$	$I(\lambda)/I(\mathrm{H}\beta)$
6583 [N II]	6.88 ± 0.30	11.83 ± 1.44	1.64 ± 0.06	5.41 ± 0.37	6.48 ± 0.31	5.14 ± 0.23	3.10 ± 0.05	0.93 ± 0.06
6678 He I	1.89 ± 0.04	...	2.69 ± 0.08	...	2.31 ± 0.24	2.64 ± 0.22	2.95 ± 0.05	2.50 ± 0.07
6717 [S II]	8.51 ± 0.36	13.97 ± 1.68	4.65 ± 0.10	13.04 ± 0.55	16.04 ± 0.40	14.92 ± 0.39	2.36 ± 0.04	2.10 ± 0.06
6731 [S II]	9.99 ± 0.33	9.02 ± 0.97	3.55 ± 0.09	8.37 ± 0.42	12.20 ± 0.35	9.95 ± 0.30	2.19 ± 0.04	1.57 ± 0.06
7065 He I	...	...	4.94 ± 0.10	2.53 ± 0.33	1.35 ± 0.19	1.90 ± 0.19	6.54 ± 0.11	2.30 ± 0.06
7136 [Ar III]	...	...	3.14 ± 0.08	3.69 ± 0.30	2.82 ± 0.20	2.33 ± 0.16	2.36 ± 0.04	1.25 ± 0.05
7281 He I	...	...	...	...	...	...	...	0.72 ± 0.03
7320 [O II]	...	...	...	...	...	...	...	0.49 ± 0.03
7330 [O II]	...	...	...	...	...	...	...	0.25 ± 0.03
$C(\mathrm{H}\beta)^a$	0.135	0.015	0.245	0.005	0.000	0.075	0.285	0.235
$F(\mathrm{H}\beta)^b$	1.98	0.42	15.97	3.05	4.21	3.55	81.87	19.30
EW(Hβ) (Å)	36.1	23.1	220.6	18.3	36.5	38.7	241.8	213.6
EW(abs) (Å)	1.15	2.00	0.80	1.25	0.65	1.30	0.65	0.60

	GALAXY						
	J2104−0035 No.2	J2104−0035 No.3	J2104−0035 No.4	J2302+0049 No.1	J2302+0049 No.2	J2324−0006	J2354−0004 No.1
3727 [O II]	114.48 ± 11.06	108.68 ± 4.99	88.02 ± 3.86	59.42 ± 1.00	190.27 ± 4.15	152.34 ± 2.43	138.52 ± 11.46
3750 H12	...	...	...	3.18 ± 0.25	...	3.14 ± 0.33	...
3771 H11	...	...	...	4.04 ± 0.23	...	3.83 ± 0.33	...
3798 H10	...	...	...	6.34 ± 0.24	...	6.29 ± 0.32	...
3820 He I	...	...	...	1.21 ± 0.14	...	...	...
3835 H9	...	...	...	7.43 ± 0.24	...	7.53 ± 0.31	...
3868 [Ne III]	...	...	...	45.23 ± 0.72	40.05 ± 1.31	47.39 ± 0.75	...
3889 He I + H8	...	16.40 ± 1.55	22.24 ± 1.54	20.52 ± 0.39	22.92 ± 1.37	21.00 ± 0.42	...
3968 [Ne III] + H7	...	17.76 ± 1.60	14.37 ± 1.37	29.75 ± 0.50	25.90 ± 1.29	31.37 ± 0.54	...
4026 He I	...	...	...	1.64 ± 0.10	...	1.84 ± 0.11	...
4068 [S II]	...	...	...	...	...	1.19 ± 0.09	...
4076 [S II]	...	...	...	...	...	0.41 ± 0.08	...
4101 Hδ	...	24.53 ± 1.22	24.61 ± 1.15	26.13 ± 0.43	30.30 ± 1.24	26.61 ± 0.45	25.66 ± 2.60
4340 Hγ	51.10 ± 3.95	49.03 ± 1.34	48.00 ± 1.33	47.28 ± 0.72	46.12 ± 1.24	47.16 ± 0.71	48.20 ± 2.01
4363 [O III]	...	3.59 ± 0.65	1.61 ± 0.69	14.90 ± 0.24	6.28 ± 0.54	9.47 ± 0.16	4.81 ± 1.57
4387 He I	...	...	...	...	...	0.31 ± 0.08	...
4471 He I	...	...	...	3.55 ± 0.09	...	3.70 ± 0.08	...
4658 [Fe III]	...	...	...	0.49 ± 0.08	...	0.59 ± 0.05	...
4686 He II	...	...	...	2.40 ± 0.08	...	0.76 ± 0.05	...
4711 [Ar IV] + He I	...	...	...	2.41 ± 0.08	...	1.10 ± 0.05	...
4740 [Ar IV]	...	...	...	1.41 ± 0.07	...	0.42 ± 0.04	...
4861 Hβ	100.00 ± 3.67	100.00 ± 2.01	100.00 ± 1.95	100.00 ± 1.45	100.00 ± 1.93	100.00 ± 1.44	100.00 ± 2.60
4921 He I	...	...	...	0.89 ± 0.05	...	1.02 ± 0.05	...
4959 [O III]	18.99 ± 1.81	32.09 ± 0.90	18.23 ± 0.62	198.50 ± 2.86	105.26 ± 1.96	182.82 ± 2.62	59.53 ± 1.82
4988 [Fe III]	...	...	...	0.75 ± 0.05	3.20 ± 0.39	0.87 ± 0.04	...
5007 [O III]	59.43 ± 2.53	94.72 ± 1.89	60.24 ± 1.23	567.92 ± 7.98	315.09 ± 5.54	543.75 ± 7.78	166.78 ± 3.88
5015 He I	...	...	...	1.78 ± 0.06	...	0.96 ± 0.05	...
5518 [Cl III]	...	...	...	...	...	0.25 ± 0.04	...
5538 [Cl III]	...	...	...	...	...	0.22 ± 0.03	...
5876 He I	5.84 ± 0.74	9.56 ± 0.57	9.39 ± 0.52	10.00 ± 0.18	8.03 ± 0.45	10.10 ± 0.16	9.03 ± 0.67
6300 [O I]	...	...	...	1.30 ± 0.05	...	2.69 ± 0.05	...
6312 [S III]	...	...	...	1.21 ± 0.06	...	1.66 ± 0.04	...
6363 [O I]	...	...	...	0.48 ± 0.04	...	0.97 ± 0.03	...
6548 [N II]	...	...	...	...	...	1.46 ± 0.04	...
6563 Hα	288.62 ± 8.99	273.23 ± 5.26	276.97 ± 5.20	277.79 ± 4.33	280.05 ± 5.31	281.56 ± 4.37	275.84 ± 6.36
6583 [N II]	4.92 ± 0.56	4.28 ± 0.38	3.93 ± 0.26	1.70 ± 0.05	6.61 ± 0.45	4.94 ± 0.09	4.85 ± 0.46
6678 He I	...	3.66 ± 0.33	2.53 ± 0.22	2.18 ± 0.05	2.49 ± 0.20	2.91 ± 0.06	...
6717 [S II]	12.66 ± 1.06	8.30 ± 0.40	8.87 ± 0.34	4.47 ± 0.08	16.91 ± 0.51	11.75 ± 0.19	12.16 ± 0.69
6731 [S II]	10.50 ± 1.04	4.19 ± 0.29	5.96 ± 0.35	3.48 ± 0.07	11.47 ± 0.39	8.79 ± 0.14	6.55 ± 0.56
7065 He I	...	...	...	2.18 ± 0.05	...	2.43 ± 0.05	...
7136 [Ar III]	...	...	...	3.41 ± 0.07	4.56 ± 0.09	5.80 ± 0.10	...
7281 He I	...	...	...	0.52 ± 0.03	...	0.59 ± 0.02	...
7320 [O II]	...	...	...	0.65 ± 0.03	...	2.06 ± 0.04	...
7330 [O II]	...	...	...	0.55 ± 0.03	...	1.67 ± 0.03	...
$C(\mathrm{H}\beta)^a$	0.015	0.225	0.205	0.260	0.195	0.250	0.080
$F(\mathrm{H}\beta)^b$	1.10	1.81	2.02	32.24	2.59	55.62	1.05
EW(Hβ) (Å)	9.6	36.3	84.2	199.4	41.9	219.5	25.0
EW(abs) (Å)	2.00	0.65	0.85	0.10	2.55	0.15	0.90

[a] zero value is assumed if a negative value is derived.

[b] in units of 10^{-16} erg s^{-1} cm^{-2}.

Table 5. Ionic and total heavy element abundances (3.6m ESO observations)

	GALAXY							
Property	J0015+0104	J0016+0108	J0029-0108	J0029-0025	J0057-0022	J0107+0001	J0109+0107	J0126-0038 No.1
T_e(O III) (K)	20000 ± 1020	17023 ± 1008	18580 ± 1188	19025 ± 1020	16258 ± 215	20000 ± 1054	12337 ± 558	14070 ± 351
T_e(O II) (K)	16284 ± 1293	15379 ± 1217	15961 ± 1470	16083 ± 1273	15006 ± 180	16284 ± 1336	12196 ± 517	13624 ± 313
O^+/H^+ ($\times10^4$)	0.084 ± 0.017	0.186 ± 0.038	0.129 ± 0.037	0.096 ± 0.019	0.199 ± 0.008	0.115 ± 0.025	0.381 ± 0.052	0.294 ± 0.020
O^{++}/H^+ ($\times10^4$)	0.033 ± 0.004	0.153 ± 0.022	0.096 ± 0.019	0.099 ± 0.013	0.200 ± 0.007	0.053 ± 0.007	0.571 ± 0.076	0.534 ± 0.036
O^{+++}/H^+ ($\times10^6$)	...	...	...	...	...	...	...	2.421 ± 0.457
O/H ($\times10^4$)	0.117 ± 0.017	0.339 ± 0.044	0.225 ± 0.042	0.194 ± 0.023	0.399 ± 0.011	0.168 ± 0.026	0.952 ± 0.092	0.852 ± 0.042
12 + log(O/H)	7.070 ± 0.063	7.530 ± 0.056	7.353 ± 0.080	7.289 ± 0.052	7.601 ± 0.012	7.226 ± 0.066	7.979 ± 0.042	7.931 ± 0.021
Ne^{++}/H^+ ($\times10^5$)	...	...	...	...	0.660 ± 0.048	...	1.498 ± 0.220	1.247 ± 0.092
ICF	...	...	...	...	1.213	...	1.155	1.141
log(Ne/O)	...	...	...	...	−0.697 ± 0.053	...	−0.740 ± 0.101	−0.777 ± 0.049
	GALAXY							
Property	J0126-0038 No.2	J0135-0023	J0213-0002 No.1	J0213-0002 No.2	J0216+0115 No.1	J0216+0115 No.2	096632	J0252+0017
T_e(O III) (K)	17255 ± 1005	18365 ± 1022	16036 ± 1017	14366 ± 1019	16076 ± 1009	17938 ± 1023	17425 ± 1005	15617 ± 1064
T_e(O II) (K)	15481 ± 1218	15895 ± 1260	14888 ± 1209	13839 ± 1182	14910 ± 1200	15750 ± 1253	15552 ± 1221	14650 ± 1256
O^+/H^+ ($\times10^4$)	0.185 ± 0.037	0.135 ± 0.028	0.169 ± 0.037	0.341 ± 0.084	0.208 ± 0.045	0.185 ± 0.038	0.249 ± 0.049	0.251 ± 0.063
O^{++}/H^+ ($\times10^4$)	0.136 ± 0.019	0.102 ± 0.014	0.263 ± 0.043	0.413 ± 0.080	0.229 ± 0.036	0.091 ± 0.013	0.078 ± 0.011	0.255 ± 0.048
O/H ($\times10^4$)	0.321 ± 0.042	0.238 ± 0.031	0.432 ± 0.057	0.754 ± 0.116	0.437 ± 0.058	0.276 ± 0.040	0.327 ± 0.051	0.506 ± 0.079
12 + log(O/H)	7.506 ± 0.057	7.376 ± 0.056	7.636 ± 0.057	7.877 ± 0.067	7.641 ± 0.057	7.441 ± 0.063	7.515 ± 0.067	7.704 ± 0.068
Ne^{++}/H^+ ($\times10^5$)	...	...	...	...	...	...	0.148 ± 0.026	...
ICF	...	...	...	...	...	...	1.408	...
log(Ne/O)	...	...	...	...	...	...	−1.195 ± 0.233	...
	GALAXY							
Property	J0256+0036	J0303-0109 No.1	J0303-0109 No.2	J0341-0026 No.1	J0341-0026 No.2	J0341-0026 No.3	G1815-6701	G2052-6912 No.1
T_e(O III) (K)	15446 ± 1004	15850 ± 960	20000 ± 1143	16136 ± 1023	17233 ± 1010	19005 ± 1014	14202 ± 308	10991 ± 110
T_e(O II) (K)	14548 ± 1183	14784 ± 816	16284 ± 1449	14942 ± 1218	15472 ± 1223	16078 ± 1264	13721 ± 273	11007 ± 105
O^+/H^+ ($\times10^4$)	0.190 ± 0.042	0.131 ± 0.020	0.121 ± 0.030	0.209 ± 0.046	0.113 ± 0.023	0.064 ± 0.013	0.318 ± 0.019	0.370 ± 0.014
O^{++}/H^+ ($\times10^4$)	0.327 ± 0.055	0.359 ± 0.055	0.046 ± 0.008	0.222 ± 0.036	0.189 ± 0.027	0.120 ± 0.015	0.645 ± 0.038	1.281 ± 0.043
O^{+++}/H^+ ($\times10^6$)	...	...	...	...	...	...	1.764 ± 0.426	0.611 ± 0.106
O/H ($\times10^4$)	0.517 ± 0.069	0.490 ± 0.059	0.166 ± 0.031	0.430 ± 0.059	0.302 ± 0.036	0.184 ± 0.020	0.981 ± 0.043	1.657 ± 0.045
12 + log(O/H)	7.713 ± 0.058	7.690 ± 0.052	7.221 ± 0.082	7.634 ± 0.059	7.480 ± 0.051	7.265 ± 0.047	7.992 ± 0.019	8.219 ± 0.012
Ne^{++}/H^+ ($\times10^5$)	0.780 ± 0.138	0.981 ± 0.159	...	...	...	...	1.645 ± 0.105	2.810 ± 0.109
ICF	1.138	1.092	...	...	...	...	1.126	1.125
log(Ne/O)	−0.765 ± 0.121	−0.660 ± 0.102	...	...	...	...	−0.724 ± 0.042	−0.720 ± 0.023
	GALAXY							
Property	G2052-6912 No.2	J2053+0039	J2105+0032 No.1	J2105+0032 No.2	J2112-0016 No.1	J2112-0016 No.2	J2119-0732	J2120-0058
T_e(O III) (K)	11865 ± 89	18364 ± 1039	17397 ± 1027	17930 ± 1021	11339 ± 320	12417 ± 771	14591 ± 1003	17281 ± 908
T_e(O II) (K)	11756 ± 83	15894 ± 1282	15541 ± 1247	15747 ± 1251	11239 ± 302	12268 ± 713	13996 ± 1167	15492 ± 736
O^+/H^+ ($\times10^4$)	0.218 ± 0.006	0.065 ± 0.014	0.089 ± 0.019	0.146 ± 0.030	0.264 ± 0.025	0.192 ± 0.036	0.183 ± 0.043	0.207 ± 0.025
O^{++}/H^+ ($\times10^4$)	1.309 ± 0.033	0.150 ± 0.021	0.194 ± 0.029	0.119 ± 0.017	1.366 ± 0.120	0.834 ± 0.151	0.487 ± 0.088	0.235 ± 0.030
O/H ($\times10^4$)	1.527 ± 0.034	0.215 ± 0.026	0.283 ± 0.035	0.265 ± 0.034	1.630 ± 0.123	1.026 ± 0.156	0.669 ± 0.098	0.442 ± 0.039
12 + log(O/H)	8.184 ± 0.009	7.332 ± 0.052	7.451 ± 0.053	7.423 ± 0.056	8.212 ± 0.033	8.011 ± 0.066	7.826 ± 0.064	7.646 ± 0.038
Ne^{++}/H^+ ($\times10^5$)	2.728 ± 0.079	...	...	...	2.871 ± 0.284	1.249 ± 0.261	1.116 ± 0.214	0.723 ± 0.093
ICF	1.064	...	...	...	1.079	1.062	1.094	1.194
log(Ne/O)	−0.721 ± 0.017	...	...	...	−0.721 ± 0.058	−0.888 ± 0.124	−0.739 ± 0.123	−0.710 ± 0.096
	GALAXY							
Property	J2150+0033	G2155-3946	J2227-0939	PHL 293B	J2310-0109 No.1	J2310-0109 No.2		
					No.1	No.2		
T_e(O III) (K)	16314 ± 1008	16087 ± 1008	14707 ± 1007	17410 ± 228	15417 ± 1005	15359 ± 1006		
T_e(O II) (K)	15036 ± 845	14915 ± 1199	14075 ± 1173	15546 ± 184	14531 ± 1183	14495 ± 867		
O^+/H^+ ($\times10^4$)	0.171 ± 0.026	0.298 ± 0.064	0.219 ± 0.051	0.053 ± 0.002	0.128 ± 0.028	0.179 ± 0.029		
O^{++}/H^+ ($\times10^4$)	0.230 ± 0.036	0.160 ± 0.025	0.434 ± 0.079	0.360 ± 0.012	0.379 ± 0.063	0.348 ± 0.059		
O^{+++}/H^+ ($\times10^6$)	...	...	...	0.655 ± 0.065	...	...		
O/H ($\times10^4$)	0.401 ± 0.044	0.458 ± 0.068	0.653 ± 0.094	0.420 ± 0.012	0.507 ± 0.069	0.527 ± 0.066		
12 + log(O/H)	7.603 ± 0.048	7.661 ± 0.065	7.815 ± 0.062	7.624 ± 0.013	7.705 ± 0.060	7.722 ± 0.054		
Ne^{++}/H^+ ($\times10^5$)	...	0.363 ± 0.070	0.993 ± 0.202	0.729 ± 0.026	0.517 ± 0.094	0.695 ± 0.127		
ICF	...	1.319	1.122	1.046	1.086	1.124		
log(Ne/O)	...	−0.980 ± 0.193	−0.768 ± 0.134	−0.742 ± 0.021	−0.956 ± 0.114	−0.829 ± 0.120		

Table 6. Ionic and Total Heavy Element Abundances (VLT observations)

	GALAXY							
Property	J0004+0025 No.1	J0004+0025 No.2	J0014−0044 No.1	J0014−0044 No.2	J0202−0047	J0301−0059 No.1	J0301−0059 No.2	J0301−0059 No.3
T_e(O III) (K)	18630 ± 1019	16701 ± 1016	13195 ± 123	16308 ± 1006	14607 ± 277	12582 ± 585	13999 ± 1236	16248 ± 1033
T_e(O II) (K)	15975 ± 1263	15229 ± 1221	12939 ± 112	15033 ± 1201	14006 ± 243	12416 ± 539	13571 ± 1104	15001 ± 1232
T_e(S III) (K)	17163 ± 846	15562 ± 844	13067 ± 102	15236 ± 835	14307 ± 230	12499 ± 485	13785 ± 1026	15186 ± 857
N_e(S II) (cm^{-3})	193 ± 128	213 ± 132	33 ± 28	167 ± 78	78 ± 38	10 ± 10	10 ± 10	10 ± 10
O^+/H^+ ($\times10^4$)	0.164 ± 0.033	0.224 ± 0.048	0.146 ± 0.005	0.274 ± 0.057	0.218 ± 0.011	0.565 ± 0.078	0.381 ± 0.089	0.300 ± 0.067
O^{++}/H^+ ($\times10^4$)	0.073 ± 0.010	0.156 ± 0.024	0.960 ± 0.027	0.158 ± 0.024	0.580 ± 0.030	0.485 ± 0.065	0.353 ± 0.084	0.141 ± 0.023
O/H ($\times10^4$)	0.237 ± 0.034	0.380 ± 0.053	1.106 ± 0.028	0.431 ± 0.062	0.798 ± 0.032	1.050 ± 0.101	0.734 ± 0.123	0.441 ± 0.071
12 + log(O/H)	7.374 ± 0.063	7.580 ± 0.061	8.044 ± 0.011	7.635 ± 0.063	7.902 ± 0.017	8.021 ± 0.042	7.866 ± 0.073	7.644 ± 0.070
N^+/H^+ ($\times10^6$)	1.015 ± 0.155	0.913 ± 0.140	0.573 ± 0.013	1.663 ± 0.240	0.811 ± 0.029	2.245 ± 0.202	2.399 ± 0.373	2.491 ± 0.409
ICF	1.377	1.675	7.041	1.534	3.647	1.892	1.930	1.408
log(N/O)	−1.229 ± 0.094	−1.396 ± 0.091	−1.438 ± 0.015	−1.228 ± 0.090	−1.431 ± 0.023	−1.393 ± 0.057	−1.200 ± 0.099	−1.099 ± 0.102
Ne^{++}/H^+ ($\times10^5$)	...	0.659 ± 0.138	1.989 ± 0.064	...	1.196 ± 0.067	1.118 ± 0.167	0.764 ± 0.198	...
ICF	...	1.273	1.047	...	1.094	1.268	1.226	...
log(Ne/O)	...	−0.656 ± 0.184	−0.725 ± 0.019	...	−0.785 ± 0.035	−0.870 ± 0.119	−0.894 ± 0.205	...
S^+/H^+ ($\times10^6$)	0.510 ± 0.059	0.484 ± 0.059	0.176 ± 0.003	0.549 ± 0.065	0.318 ± 0.010	0.988 ± 0.076	0.920 ± 0.121	1.038 ± 0.138
S^{++}/H^+ ($\times10^6$)	...	...	1.393 ± 0.056	...	1.036 ± 0.079	0.919 ± 0.113	...	...
ICF	...	...	1.724	...	1.142	0.897	...	...
log(S/O)	...	...	−1.612 ± 0.019	...	−1.712 ± 0.031	−1.788 ± 0.052	...	...
Cl^{++}/H^+ ($\times10^8$)	...	...	3.474 ± 0.410	...	...	...	...	...
ICF	...	...	1.243	...	...	...	...	...
log(Cl/O)	...	...	−3.408 ± 0.052	...	...	...	...	...
Ar^{++}/H^+ ($\times10^7$)	...	...	3.416 ± 0.075	...	3.606 ± 0.116	3.719 ± 0.336	3.569 ± 0.440	...
Ar^{+++}/H^+ ($\times10^7$)	...	...	1.213 ± 0.103	...	...	...	...	...
ICF	...	...	1.122	...	1.141	1.097	1.043	...
log(Ar/O)	...	...	−2.460 ± 0.020	...	−2.287 ± 0.022	−2.410 ± 0.057	−2.295 ± 0.090	...
Fe^{++}/H^+($\times10^6$)(4658)	...	...	...	...	...	...	...	...
Fe^{++}/H^+($\times10^6$)(4988)	...	...	0.125 ± 0.003	...	...	...	...	...
ICF	...	...	10.398	...	...	...	...	...
log(Fe/O) (λ4658)	...	...	...	...	...	...	...	...
log(Fe/O) (4988)	...	...	−1.932 ± 0.015	...	...	...	...	...

	GALAXY							
Property	J0315−0024 No.1	J0315−0024 No.2	J0338+0013	G0405-3648 No.1	G0405-3648 No.2	G0405-3648 No.3	J0519+0007	J2104−0035 No.1
T_e(O III) (K)	12550 ± 1733	18111 ± 1012	17882 ± 208	15013 ± 1293	18169 ± 908	21295 ± 1349	20143 ± 238	20194 ± 294
T_e(O II) (K)	12387 ± 1597	15811 ± 1243	15729 ± 165	14278 ± 1125	15830 ± 712	16407 ± 902	16306 ± 171	16313 ± 210
T_e(S III) (K)	12468 ± 1438	16732 ± 840	16542 ± 173	14645 ± 1073	16780 ± 753	19375 ± 1119	18419 ± 198	18461 ± 244
N_e(S II) (cm^{-3})	1099 ± 206	10 ± 10	116 ± 50	10 ± 10	108 ± 57	10 ± 10	483 ± 60	84 ± 74
O^+/H^+ ($\times10^4$)	0.339 ± 0.138	0.147 ± 0.030	0.048 ± 0.002	0.137 ± 0.030	0.125 ± 0.014	0.107 ± 0.014	0.021 ± 0.001	0.019 ± 0.001
O^{++}/H^+ ($\times10^4$)	0.289 ± 0.115	0.108 ± 0.014	0.385 ± 0.012	0.228 ± 0.051	0.099 ± 0.012	0.069 ± 0.010	0.248 ± 0.007	0.162 ± 0.006
O^{+++}/H^+ ($\times10^6$)	...	...	0.531 ± 0.042	...	...	...	0.444 ± 0.021	0.126 ± 0.019
O/H ($\times10^4$)	0.628 ± 0.179	0.255 ± 0.033	0.438 ± 0.012	0.365 ± 0.059	0.224 ± 0.018	0.176 ± 0.017	0.273 ± 0.007	0.183 ± 0.006
12 + log(O/H)	7.798 ± 0.124	7.406 ± 0.056	7.641 ± 0.012	7.562 ± 0.070	7.351 ± 0.036	7.246 ± 0.043	7.437 ± 0.012	7.261 ± 0.014
N^+/H^+ ($\times10^6$)	0.768 ± 0.202	0.786 ± 0.128	0.110 ± 0.004	0.440 ± 0.067	0.430 ± 0.036	0.319 ± 0.031	0.195 ± 0.004	0.058 ± 0.003
ICF	1.847	1.713	8.642	2.686	1.785	1.616	12.223	8.833
log(N/O)	−1.646 ± 0.169	−1.277 ± 0.091	−1.662 ± 0.019	−1.490 ± 0.096	−1.465 ± 0.051	−1.535 ± 0.061	−1.059 ± 0.015	−1.551 ± 0.029
Ne^{++}/H^+ ($\times10^5$)	0.416 ± 0.199	...	0.689 ± 0.022	0.258 ± 0.071	0.185 ± 0.028	0.164 ± 0.024	0.447 ± 0.013	0.301 ± 0.011
ICF	1.240	...	1.040	1.143	1.251	1.286	1.031	1.037
log(Ne/O)	−1.085 ± 0.385	...	−0.786 ± 0.019	−1.094 ± 0.181	−0.987 ± 0.123	−0.923 ± 0.133	−0.774 ± 0.018	−0.766 ± 0.022
S^+/H^+ ($\times10^6$)	0.291 ± 0.066	0.202 ± 0.028	0.073 ± 0.002	0.225 ± 0.028	0.250 ± 0.016	0.205 ± 0.016	0.040 ± 0.001	0.031 ± 0.001
S^{++}/H^+ ($\times10^6$)	...	...	0.387 ± 0.027	...	...	...	0.223 ± 0.009	0.189 ± 0.019
ICF	...	...	1.947	...	...	...	2.539	1.978
log(S/O)	...	...	−1.689 ± 0.028	...	...	...	−1.612 ± 0.018	−1.623 ± 0.040
Ar^{++}/H^+ ($\times10^7$)	...	...	1.068 ± 0.028	1.544 ± 0.201	0.937 ± 0.080	0.618 ± 0.052	0.682 ± 0.014	0.357 ± 0.015
Ar^{+++}/H^+ ($\times10^7$)	...	...	0.919 ± 0.051	...	...	...	0.762 ± 0.032	0.371 ± 0.049
ICF	...	...	1.867	1.058	1.048	1.060	2.455	1.898
log(Ar/O)	...	...	−2.342 ± 0.027	−2.349 ± 0.090	−2.358 ± 0.051	−2.430 ± 0.056	−2.213 ± 0.025	−2.431 ± 0.064
Fe^{++}/H^+($\times10^6$)(4658)	...	...	0.083 ± 0.010	...	...	...	0.076 ± 0.007	...
Fe^{++}/H^+($\times10^6$)(4988)	...	...	0.091 ± 0.009	...	0.327 ± 0.059	...	0.101 ± 0.007	0.117 ± 0.021
ICF	...	...	12.634	...	2.360	...	18.224	12.932
log(Fe/O) (λ4658)	...	...	−1.623 ± 0.054	...	...	...	−1.298 ± 0.041	...
log(Fe/O) (4988)	...	...	−1.579 ± 0.043	...	−1.464 ± 0.086	...	−1.170 ± 0.031	−1.081 ± 0.079

	GALAXY						
Property	J2104−0035 No.2	J2104−0035 No.3	J2104−0035 No.4	J2302+0049 No.1	J2302+0049 No.2	J2324−0006	J2354−0004 No.1
T_e(O III) (K)	20000 ± 1061	21471 ± 2559	17794 ± 4091	17281 ± 179	15203 ± 616	14313 ± 128	18120 ± 3255
T_e(O II) (K)	16284 ± 1345	16411 ± 1693	15697 ± 3257	15492 ± 145	14399 ± 533	13801 ± 113	15814 ± 2559
T_e(S III) (K)	18300 ± 880	19521 ± 2124	16469 ± 3396	16043 ± 148	14801 ± 511	14057 ± 106	16740 ± 2702
N_e(S II) (cm^{-3})	255 ± 248	10 ± 10	10 ± 10	143 ± 44	10 ± 10	84 ± 31	10 ± 10

Table 6. continued.

O^+/H^+ ($\times10^4$)	0.083 ± 0.018	0.075 ± 0.019	0.070 ± 0.036	0.050 ± 0.001	0.196 ± 0.020	0.182 ± 0.005	0.107 ± 0.044
O^{++}/H^+ ($\times10^4$)	0.034 ± 0.004	0.047 ± 0.012	0.043 ± 0.024	0.450 ± 0.012	0.335 ± 0.035	0.675 ± 0.018	0.120 ± 0.051
O^{+++}/H^+ ($\times10^6$)	...	...	...	1.342 ± 0.062	...	0.715 ± 0.051	...
O/H ($\times10^4$)	0.117 ± 0.019	0.122 ± 0.023	0.113 ± 0.043	0.513 ± 0.012	0.531 ± 0.041	0.864 ± 0.019	0.227 ± 0.067
12 + log(O/H)	7.068 ± 0.070	7.088 ± 0.080	7.052 ± 0.166	7.710 ± 0.010	7.725 ± 0.033	7.937 ± 0.009	7.355 ± 0.128
N^+/H^+ ($\times10^6$)	0.310 ± 0.051	0.266 ± 0.049	0.265 ± 0.095	0.117 ± 0.003	0.528 ± 0.045	0.431 ± 0.009	0.322 ± 0.092
ICF	1.323	1.592	1.587	9.717	2.732	4.662	2.133
log(N/O)	−1.455 ± 0.103	−1.462 ± 0.114	−1.428 ± 0.230	−1.653 ± 0.017	−1.566 ± 0.049	−1.633 ± 0.013	−1.518 ± 0.177
Ne^{++}/H^+ ($\times10^5$)	...	...	...	0.819 ± 0.024	1.030 ± 0.115	1.457 ± 0.043	...
ICF	...	...	...	1.040	1.139	1.072	...
log(Ne/O)	...	...	...	−0.780 ± 0.017	−0.656 ± 0.075	−0.743 ± 0.018	...
S^+/H^+ ($\times10^6$)	0.198 ± 0.026	0.103 ± 0.015	0.132 ± 0.038	0.073 ± 0.001	0.293 ± 0.018	0.232 ± 0.004	0.164 ± 0.037
S^{++}/H^+ ($\times10^6$)	...	...	...	0.508 ± 0.027	...	1.045 ± 0.032	...
ICF	...	...	...	2.124	...	1.300	...
log(S/O)	...	...	...	−1.619 ± 0.023	...	−1.716 ± 0.014	...
Cl^{++}/H^+ ($\times10^8$)	...	...	...	...	...	1.385 ± 0.150	...
ICF	...	...	...	...	...	1.193	...
log(Cl/O)	...	...	...	...	...	−3.719 ± 0.048	...
Ar^{++}/H^+ ($\times10^7$)	...	...	...	1.222 ± 0.027	1.869 ± 0.095	2.613 ± 0.053	...
Ar^{+++}/H^+ ($\times10^7$)	...	...	...	1.004 ± 0.053	...	0.487 ± 0.052	...
ICF	...	...	...	2.041	1.061	1.265	...
log(Ar/O)	...	...	...	−2.313 ± 0.024	−2.428 ± 0.040	−2.417 ± 0.015	...
Fe^{++}/H^+($\times10^6$)(4658)	...	...	...	0.086 ± 0.014	...	0.139 ± 0.012	...
Fe^{++}/H^+($\times10^6$)(4988)	...	...	...	0.131 ± 0.010	0.673 ± 0.096	0.204 ± 0.010	...
ICF	...	...	...	14.309	3.639	6.495	...
log(Fe/O) (λ4658)	...	...	...	−1.618 ± 0.069	...	−1.982 ± 0.039	...
log(Fe/O) (4988)	...	...	...	−1.437 ± 0.034	−1.336 ± 0.071	−1.815 ± 0.024	...

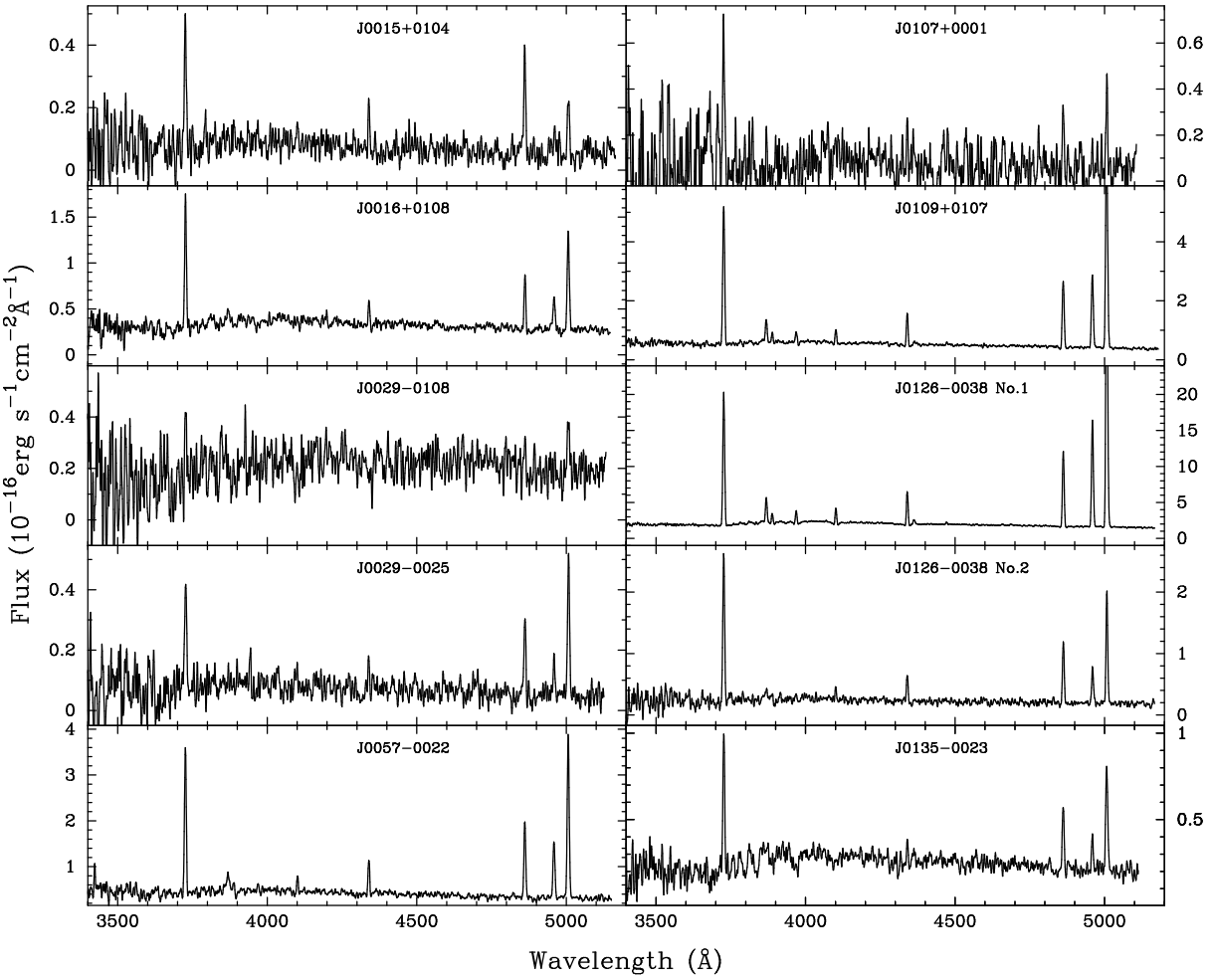

Fig. 1. The flux-calibrated and redshift-corrected 3.6m ESO telescope spectra of the emission-line galaxies.

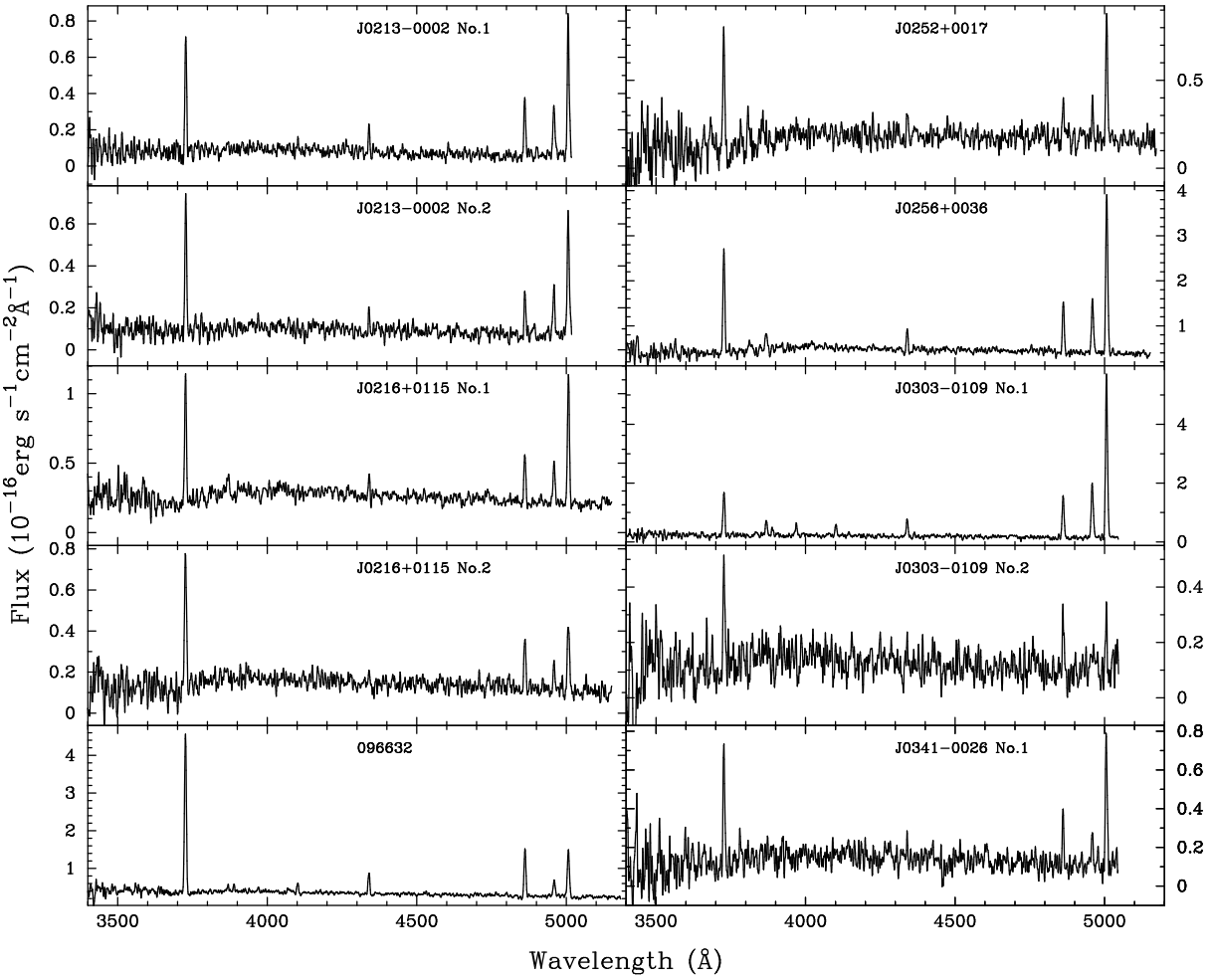

Fig. 1. *–Continued*

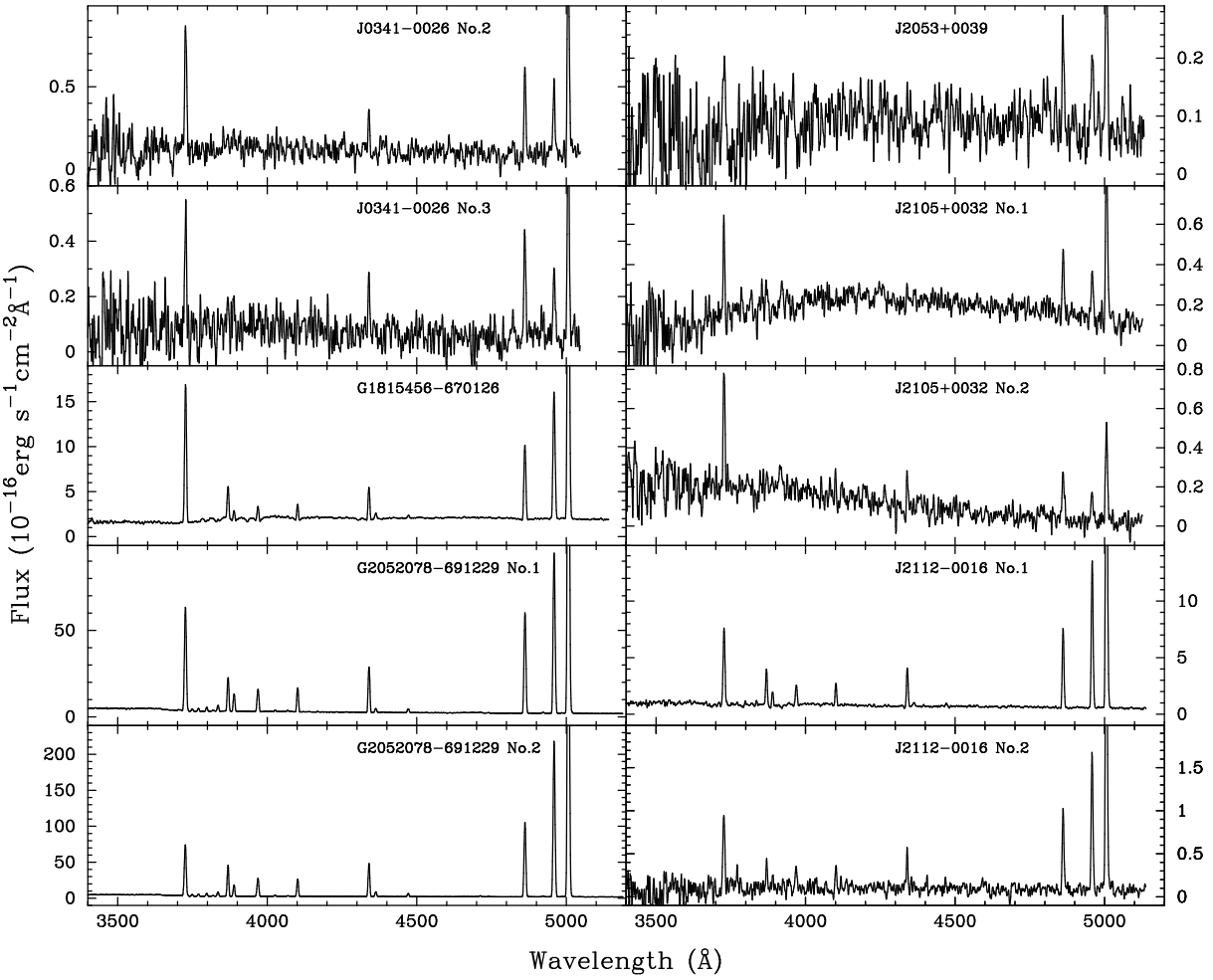

Fig. 1. *–Continued*

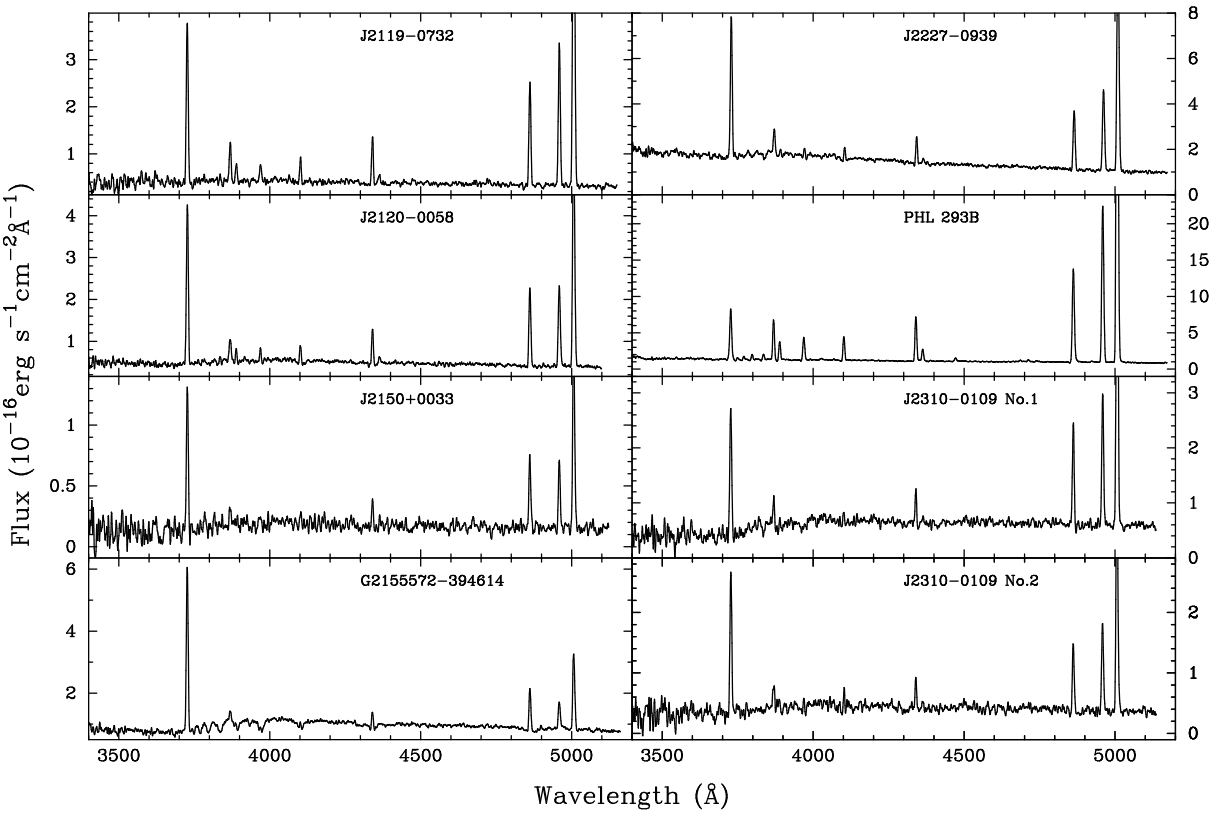

Fig. 1. –*Continued*

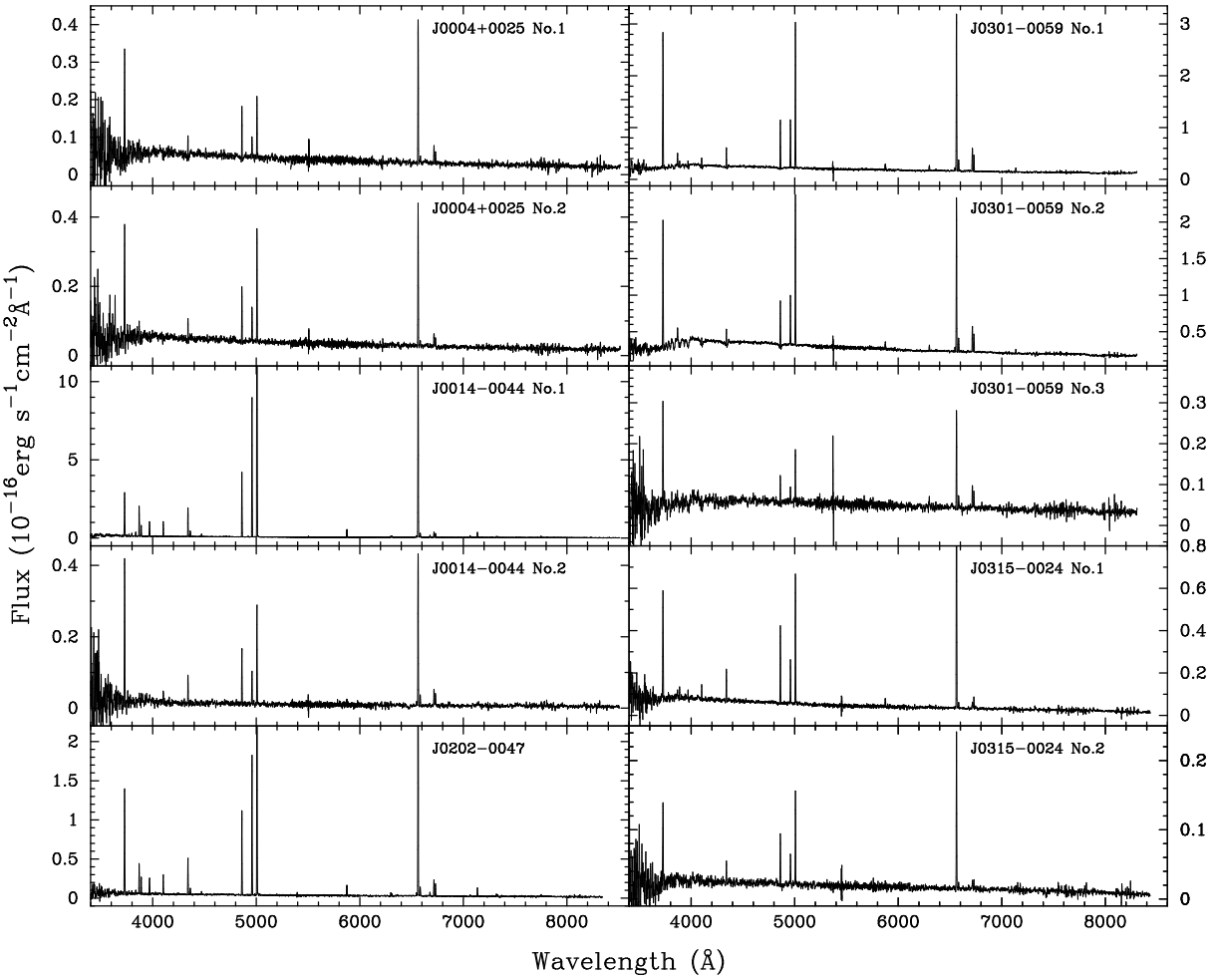

Fig. 2. The flux-calibrated and redshift-corrected VLT spectra of the emission-line galaxies.

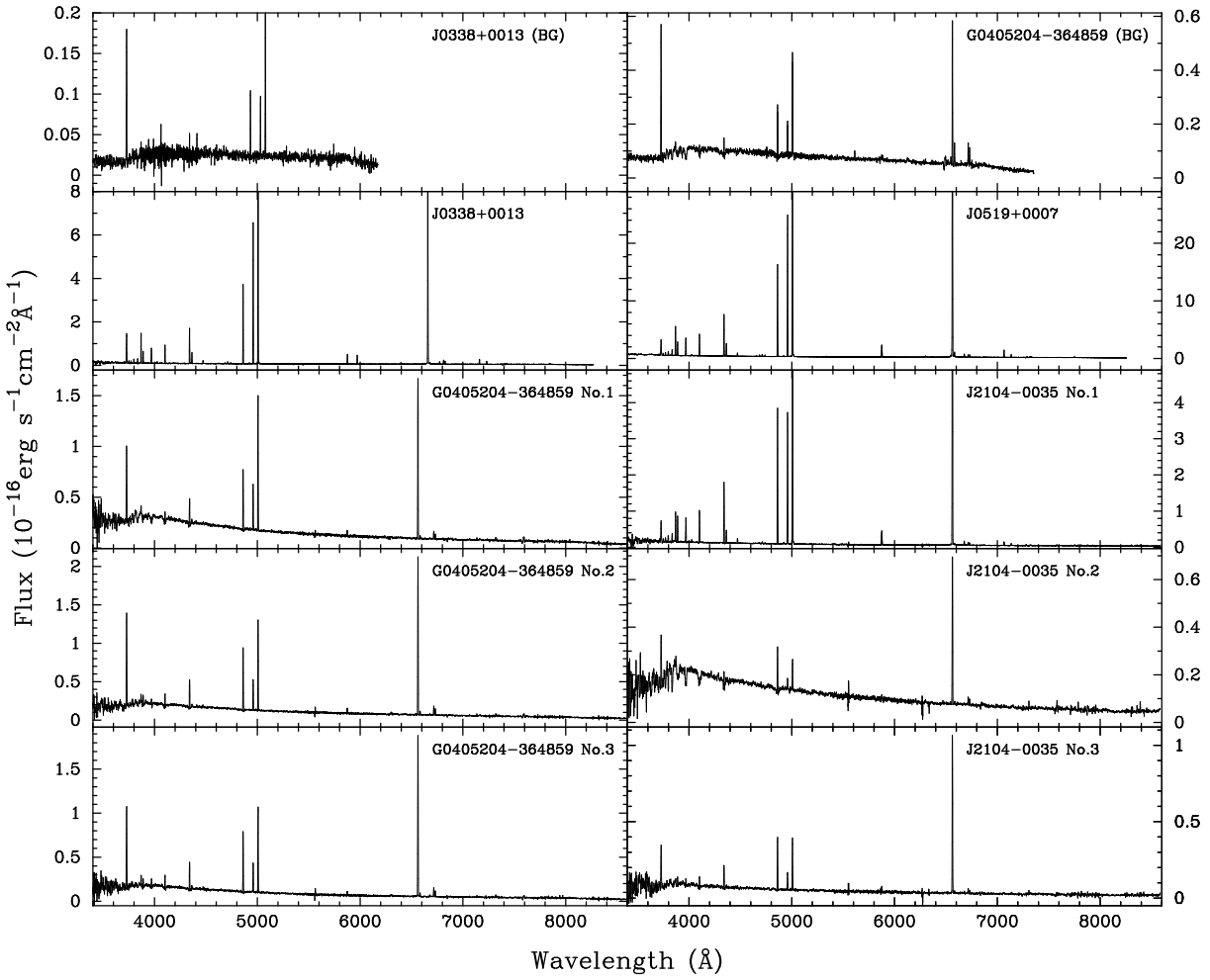

Fig. 2. –*Continued*

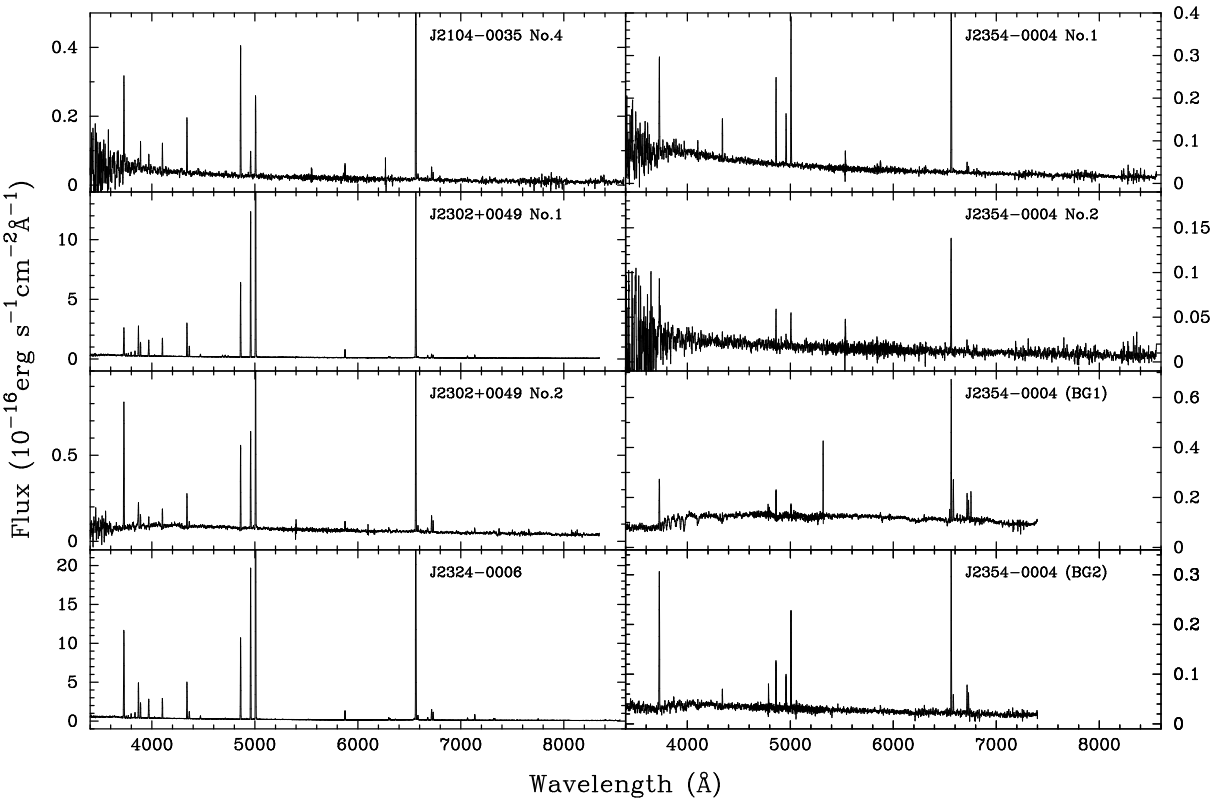

Fig. 2. *–Continued*